

Modeling complex measurement error in microbiome experiments

David S Clausen

Department of Biostatistics, University of Washington
and

Amy D Willis*

Department of Biostatistics, University of Washington

28 April 2022

Abstract

The relative abundances of species in a microbiome is a scientifically important parameter to estimate given the critical role that microbiomes play in human and environmental health. However, data from artificially constructed microbiomes shows that measurement error may induce substantial bias in common estimators of this quantity. To address this, we propose a semiparametric model that accounts for common forms of measurement error in microbiome experiments. Notably, our model allows relative abundances to lie on the boundary of the simplex. We present a stable algorithm for computing parameter estimates, asymptotically valid procedures for inference in this nonstandard problem, and examples of the utility of the method. Our approach can be used to select or compare experimental protocols, design experiments with appropriate control data, analyze mixed-specimen samples, and remove across-sample contamination.

Keywords: constrained estimation; boundary problems; non-standard parameter space; semiparametric modeling; high-throughput sequencing; genomics

*The authors gratefully acknowledge support from the National Institute of General Medical Sciences (R35 GM133420); the University of Washington Cystic Fibrosis Foundation Research Development Program; the National Institute of Environmental Health Sciences (T32 ES015459); and the Seattle Chapter of the ARCS Foundation. The opinions expressed in this article are those of the authors and do not necessarily represent the official views of the NIGMS, the NIEHS, the Cystic Fibrosis Foundation, or the ARCS Foundation. The authors are grateful to Michael McLaren and Benjamin Callahan for helpful discussions about model specification, and to Pauline Trinh for bioinformatics support.

1 Introduction

In the past two decades, next-generation sequencing (NGS) methods have improved the characterization of complex microbial communities. Microbial communities, or microbiomes, are present in the human body (including in the digestive, urogenital and pulmonary tracts) as well as natural environments such as soils, salt- and freshwater systems, and aquifers. While NGS methods are able to detect and characterize a wide variety of microscopic organisms, measurements taken via these methods are subject to substantial distortion compared to the communities they represent (Nearing et al., 2021; Pollock et al., 2018; Sinha et al., 2017; Clausen and Willis, 2021).

Numerous approaches have been proposed to address measurement error in high-throughput sequencing studies. A particularly common concern are “batch effects,” which are systemic distortions in observed abundance data due either to true biological variation (e.g., cage/tank effects in model organism studies) or measurement error (e.g., lot-to-lot variation in reagents). The majority of batch effect methods used in microbiome studies were originally developed for RNA-seq and microarray analysis, such as surrogate variable analysis (Leek and Storey, 2007), ComBat (Johnson et al., 2007), remove unwanted variation (Gagnon-Bartsch and Speed, 2012) and batch mean centering (Sims et al., 2008). Batch effects methods developed specifically for microbiome studies include percentile-normalization for case-control meta-analyses (Gibbons et al., 2018), and a Bayesian multinomial-Dirichlet model (Dai et al., 2019).

Another line of research aims to directly estimate microbial abundances from sequencing data. In an early effort in this area, Brooks et al. (2015), fit linear models to model the empirical proportions of bacteria in communities of known composition. However, the complexity of these models, which incorporated second-order species interactions, limited their generalizability and interpretability. Using data published by Brooks et al. (2015), McLaren et al. (2019) proposed a parsimonious model for microbial abundance data in which observed ratios of bacterial strains are multiplicatively distorted due to the over-detection of some strains relative to others. This approach yielded improved predictive performance, particularly in the form of cross-sample generalizability, as it was able to disentangle measurement protocol effects from sample composition. Generalizing this approach remains an active area of research, and multiple methods now exist to estimate

multiplicative detection effects (Silverman et al., 2021; Zhao and Satten, 2021).

Alas, unequal detection of bacterial strains is not the only impediment to estimating microbial abundances from NGS data. Contamination introduced during sample handling, preparation and sequencing can be a significant source of measurement error, particularly in low biomass settings (Willner et al., 2012; Salter et al., 2014; Weiss et al., 2014). Methods to identify and remove contamination include SourceTracker (Knights et al., 2011) and FEAST (Shenhav et al., 2019), which model contamination as a mixture of contributions from an arbitrary number of known sources in addition to a single unknown source. Another method, decontam (Davis et al., 2018), uses measured DNA concentrations to identify contaminants under the assumption that total contaminant DNA concentration is approximately constant across samples.

In this paper, we develop a method to account both for systematic over- and under-detection of taxa as well as contamination in NGS data. The framework we present allows for principled inclusion of covariates governing both detection effects and contamination, such as batch covariates. We develop a stable algorithm for constrained estimation of relative abundance and measurement error parameters, and present inferential procedures that remain valid when relative abundance parameters lie on the boundary of the parameter space. We demonstrate applications of our method to relative abundance estimation under complex measurement error, and to model evaluation and hypothesis testing in cross-protocol measurement experiments. We show consistency of our estimators under mild conditions and empirically evaluate its performance on a dataset of measurements on specimens of known composition and under simulation. We conclude with a discussion of advantages of our approach and areas for future research.

2 A measurement error model for microbiome data

We propose a measurement error model that accounts for both contaminant reads and taxon-dependent distortion of sample community structure. We use the term “read” as a catch-all for the measurement output of microbiome sequencing experiments, but do not require that observations be integer-valued. Similarly, “sample” refers to the unit of sequencing; “specimen” refers to a unique source of genetic material that may be repeatedly sampled for sequencing; and “taxon”

refers to a grouping of organisms (e.g., species, strains or cell types).

Let $W_i = (W_{i1}, \dots, W_{iJ})$ denote observed reads from taxa $1, \dots, J$ in sample i . A common modeling assumption for high-throughput sequencing data is

$$\mathbb{E}[W_i | \mathbf{p}_i, \gamma_i] = \exp(\gamma_i) \mathbf{p}_i \quad (1)$$

where $\mathbf{p}_i \in \mathbb{S}^{J-1}$ is the unknown relative abundances of taxa $1, \dots, J$ and $\exp(\gamma_i) \in \mathbb{R}^+$ is a sampling intensity parameter (throughout, we let \mathbb{S}^{J-1} denote the closed $J - 1$ -dimensional simplex). While the simplicity of this model is appealing, it poorly describes actual microbiome sequencing data because taxa are not all detected equally well (McLaren et al., 2019). To account for this, we begin by considering the model

$$\mathbb{E}[W_i | \mathbf{p}_i, \beta, \gamma_i] = \exp(\gamma_i) (\exp(\beta) \circ \mathbf{p}_i) \quad (2)$$

where $\beta = \beta_1, \dots, \beta_J$ represents the detection effects for taxa $1, \dots, J$ in a given experiment (\circ indicates element-wise multiplication). As an identifiability constraint, we set $\beta_J = 0$, and so interpret $\exp(\beta_j), j = 1, \dots, J$, as the degree of multiplicative over- or under-detection of taxon j relative to taxon J .

We now generalize model (2) to multiple samples and one or more experimental protocols. For a study involving n samples of K unique sources of samples ($n \geq K$), we define the *sample design matrix* $\mathbf{Z} \in \mathbb{R}^{n \times K}$ to link samples to specimens. In most experiments, $Z_{ik} = \mathbf{1}_{\{\text{sample } i \text{ taken from specimen } k\}}$, but we note that more complex designs are possible. For example, if sample i is a 1 : 1 mixture of microbial communities k and k' , we may specify $Z_{ik} = Z_{ik'} = \frac{1}{2}$. Letting \mathbf{p} be a $K \times J$ matrix such that the k -th row of \mathbf{p} gives the true relative abundances of taxa in specimen k , we have that the relative abundance vector for sample i is $(\mathbf{Zp})_{i\cdot}$. To reflect that a sample's relative abundance must be a convex combination of sources' relative abundances, we require $\mathbf{Z}_{i\cdot} \in \mathbb{S}^{K-1}$. We allow differing detections across samples to be specified via the *detection design matrix* $\mathbf{X} \in \mathbb{R}^{n \times p}$. For example, if samples are processed using one of p different protocols, we might specify $X_{iq} = \mathbf{1}_{\{\text{sample } i \text{ processed with protocol } q\}}$. Accordingly, we now consider a detection effect matrix $\beta \in \mathbb{R}^{p \times J}$. As above, we impose identifiability constraint $\beta_{\cdot J} = \mathbf{0}_p$. Therefore, one

generalization of model (2) is

$$\mathbb{E}[\text{reads due to contributing samples}|\boldsymbol{\beta}, \mathbf{p}, \boldsymbol{\gamma}, \mathbf{Z}, \mathbf{X}] = \mathbf{D}_\gamma(\mathbf{Zp}) \circ \exp(\mathbf{X}\boldsymbol{\beta}), \quad (3)$$

where $\mathbf{D}_\gamma = \text{diag}(\exp(\boldsymbol{\gamma}))$, and where exponentiation is element-wise.

We now extend this model to reflect contributions of contaminant sources to the expected number of observed reads. We consider \tilde{K} sources of contamination with relative abundance profiles given in the rows of $\tilde{\mathbf{p}} \in \mathbb{R}^{\tilde{K} \times J}$. To link sources of contamination to samples, we let $\tilde{\mathbf{Z}} \in \mathbb{R}^{n \times \tilde{K}}$ be a *spurious read design* matrix. Most commonly we expect $\tilde{Z}_{i\tilde{k}} = \mathbf{1}_{\{\text{source } \tilde{k} \text{ may contribute reads to sample } i\}}$, but we give an example of an analysis with more complex $\tilde{\mathbf{Z}}$ in Section 5.2. Then, along with contaminant read intensities $\tilde{\boldsymbol{\gamma}} = [\tilde{\gamma}_1, \dots, \tilde{\gamma}_{\tilde{K}}]^\text{T}$, we propose to model

$$\mathbb{E}[\text{reads due to spurious sources}|\boldsymbol{\gamma}, \tilde{\boldsymbol{\gamma}}, \tilde{\mathbf{p}}, \tilde{\mathbf{Z}}] = \mathbf{D}_\gamma \tilde{\mathbf{Z}} [\tilde{\mathbf{p}} \circ \exp(\tilde{\boldsymbol{\gamma}} \mathbf{1}_J^\text{T})]. \quad (4)$$

While we could incorporate a detection design matrix for contaminant reads (replacing (4) with $\mathbf{D}_\gamma \tilde{\mathbf{Z}} [\tilde{\mathbf{p}} \circ \exp(\tilde{\boldsymbol{\gamma}} \mathbf{1}_J^\text{T} + \tilde{\mathbf{X}}\boldsymbol{\beta})]$ for $\tilde{\mathbf{X}} \in \mathbb{R}^{\tilde{K} \times p}$), for most practical applications it is sufficient to identify $\tilde{\mathbf{p}}$ up to detection distortion. Therefore, combining models (3) and (4), we propose the following mean model for next-generation sequencing data $\mathbf{W} \in \mathbb{R}^{n \times J}$:

$$\boldsymbol{\mu} := \mathbb{E}[\mathbf{W}|\boldsymbol{\beta}, \mathbf{p}, \boldsymbol{\gamma}, \tilde{\mathbf{p}}, \tilde{\boldsymbol{\gamma}}] = \mathbf{D}_\gamma(\mathbf{Zp}) \circ \exp(\mathbf{X}\boldsymbol{\beta}) + \mathbf{D}_\gamma \tilde{\mathbf{Z}} [\tilde{\mathbf{p}} \circ \exp(\tilde{\boldsymbol{\gamma}} \mathbf{1}_J^\text{T})]. \quad (5)$$

3 Estimation and optimization

We propose to estimate parameters $\boldsymbol{\theta}^* := (\boldsymbol{\theta}, \boldsymbol{\gamma}) := (\boldsymbol{\beta}, \mathbf{p}, \tilde{\mathbf{p}}, \tilde{\boldsymbol{\gamma}}, \boldsymbol{\gamma})$ either by maximum likelihood or by maximum weighted likelihood. We use likelihoods to define M-estimators and do not require or assume that the distribution of \mathbf{W} lies in any particular parametric class. We show consistency of and outline weak convergence results for our estimators of $\boldsymbol{\theta} := (\boldsymbol{\beta}, \mathbf{p}, \tilde{\mathbf{p}}, \tilde{\boldsymbol{\gamma}})$ under mild conditions in Supporting Information (SI) Section 2. Note that elements of $\boldsymbol{\gamma} \in \mathbb{R}^n$ are sample-specific nuisance parameters. We use $\boldsymbol{\theta}_0$ to denote the true value of $\boldsymbol{\theta}$. Our unweighted objective is given by a Poisson log-likelihood:

$$M_n^*(\boldsymbol{\theta}^*) := \frac{1}{n} l_n(\boldsymbol{\theta}^*) = \frac{1}{n} \mathbf{1}^\text{T} [\text{vec}(\mathbf{W}) \circ \log(\text{vec}(\boldsymbol{\mu}(\boldsymbol{\theta}^*))) - \text{vec}(\boldsymbol{\mu}(\boldsymbol{\theta}^*))]. \quad (6)$$

We use $M_n(\boldsymbol{\theta})$ to indicate the profile log-likelihood $\sup_{\boldsymbol{\gamma} \in \mathbb{R}^n} M_n^*(\boldsymbol{\theta}, \boldsymbol{\gamma})$. Consistency of the maximum likelihood estimate $\hat{\boldsymbol{\theta}}$ for $\boldsymbol{\theta}_0$ does not require W_{ij} to follow a Poisson distribution. However, the Poisson estimator will in general be inefficient if the relationship between $\mathbb{E}[W_{ij}|Z_i, X_i, \tilde{Z}_i, \gamma_i, \boldsymbol{\theta}_0]$ and $\text{Var}[W_{ij}|Z_i, X_i, \tilde{Z}_i, \gamma_i, \boldsymbol{\theta}_0]$ is not linear (McCullagh, 1983). Therefore, to obtain a more efficient estimator, we also consider maximizing a reweighted Poisson log-likelihood, with weights chosen on the basis of a flexibly estimated mean-variance relationship. We motivate our specific choice of weights via the Poisson score equations (see SI Section 1). For weighting vector $\hat{\mathbf{v}} \in \mathbb{R}_+^{nJ}$ such that $\mathbf{1}^T \hat{\mathbf{v}} = nJ$, we define the weighted Poisson log-likelihood as

$$M_n^{\star \hat{\mathbf{v}}}(\boldsymbol{\theta}^*) := \frac{1}{n} \hat{\mathbf{v}}^T [\text{vec}(\mathbf{W}) \circ \log(\text{vec}(\boldsymbol{\mu}(\boldsymbol{\theta}^*))) - \text{vec}(\boldsymbol{\mu}(\boldsymbol{\theta}^*))]. \quad (7)$$

We define $M_n^{\hat{\mathbf{v}}n}(\boldsymbol{\theta})$ by analogy with $M_n(\boldsymbol{\theta})$ above. We select $\hat{\mathbf{v}}$ via a centered isotonic regression (Oron and Flournoy, 2017) of squared residuals $\text{vec}[(\mathbf{W} - \hat{\boldsymbol{\mu}})^2]$ on fitted means $\text{vec}[\hat{\boldsymbol{\mu}}]$ obtained from the unweighted objective. Full details are given in SI Section 1, but briefly, we set $\hat{v}_{ij} \propto \frac{\hat{\mu}_{ij} + 1}{\hat{\sigma}_{ij}^2 + 1}$, where $\hat{\sigma}_{ij}^2$ is the monotone regression fitted value for μ_{ij} .

Computing maximum (weighted) likelihood estimates of $\boldsymbol{\theta}^*$ is a constrained optimization problem, as the relative abundance parameters in our model are simplex-valued, and the estimate may lie on the boundary of the simplex. Therefore, we minimize $f_n(\boldsymbol{\theta}^*) = -M_n^*(\boldsymbol{\theta}^*)$ or $f_n(\boldsymbol{\theta}^*) = -M_n^{\hat{\mathbf{v}}n}(\boldsymbol{\theta}^*)$ in two steps. In the first step, we employ the barrier method, converting our constrained optimization problem into a sequence of unconstrained optimizations, permitting solutions progressively closer to the boundary. That is, for barrier penalty parameter t , we update $\boldsymbol{\theta}$ as

$$\boldsymbol{\theta}^{*(r+1)} = \arg \min_{\boldsymbol{\theta}} \left(f_n(\boldsymbol{\theta}^*) + \frac{1}{t^{(r)}} \left[\sum_{k=1}^K \sum_{j=1}^J -\log p_{kj} + \sum_{\tilde{k}=1}^{\tilde{K}} \sum_{j=1}^J -\log \tilde{p}_{\tilde{k}j} \right] \right) \quad (8)$$

$$\text{subject to } \sum_{j=1}^J p_{kj} = 1 \text{ and } \sum_{j=1}^J \tilde{p}_{\tilde{k}j} = 1 \text{ for all } k, \tilde{k} \text{ s.t. } \mathbf{p}_k, \tilde{\mathbf{p}}_{\tilde{k}} \text{ unknown} \quad (9)$$

and set $t^{(r+1)} = at^{(r)}$ where $a > 1$ is a prespecified incrementing factor, iterating until $t^{(r)} > t_{\text{cutoff}}$ for large t_{cutoff} . In practice we find that $t^{(0)} = 1$, $a = 10$, and $t_{\text{cutoff}} = 10^{12}$ yield good performance. We enforce the sum-to-one constraints (9) by reparametrizing \mathbf{p} and $\tilde{\mathbf{p}}$ as $\boldsymbol{\rho}$ and $\tilde{\boldsymbol{\rho}}$, with $\rho_{kj} := \log \frac{p_{kj}}{p_{kJ}}$ and $\tilde{\rho}_{\tilde{k}j} := \log \frac{\tilde{p}_{\tilde{k}j}}{\tilde{p}_{\tilde{k}J}}$ for $j = 1, \dots, J-1$, which are well-defined because of the logarithmic penalty terms in (8).

In the second step of our optimization procedure, we apply a constrained Newton algorithm within an augmented Lagrangian algorithm to allow elements of $\hat{\mathbf{p}}$ and $\hat{\hat{\mathbf{p}}}$ to equal zero. Iteratively in each row \mathbf{p}_k of \mathbf{p} , we approximately solve

$$\arg \min_{\mathbf{p}_k} f_n(\mathbf{p}_k) \quad \text{subject to} \quad \sum_{j=1}^J p_{kj} = 1, \quad p_{kj} \geq 0 \text{ for } j = 1, \dots, J \quad (10)$$

where $f_n(\mathbf{p}_k)$ is the objective function f_n considered as a function of only \mathbf{p}_k , with all other parameters fixed at values obtained in previous optimization steps. To do this, we choose update directions for \mathbf{p}_k via an augmented Lagrangian algorithm of Bazaraa (2006) applied to

$$\mathcal{L}_k := Q_k^{(t)} + \nu \left[\sum_{j=1}^J p_{kj} - 1 \right] + \mu \left[\sum_{j=1}^J p_{kj} - 1 \right]^2 \quad (11)$$

where $Q_k^{(t)}$ is a quadratic approximation to $f_n(\mathbf{p}_k)$ at $\mathbf{p}_k^{(t)}$ and ν and μ are chosen using the algorithm of Bazaraa (2006). The augmented Lagrangian algorithm iteratively updates ν and μ until solutions to \mathcal{L}_k satisfy $|\sum_{j=1}^J p_{kj} - 1| < \epsilon$ for a small prespecified value of ϵ (we use 10^{-10} by default). Within each iteration of the augmented Lagrangian algorithm, we minimize \mathcal{L}_k via fast non-negative least squares to preserve nonnegativity of \mathbf{p}_k . Through the augmented Lagrangian algorithm, we obtain a value $\mathbf{p}_{\mathcal{L}_k}^{(t)}$ of \mathbf{p}_k that minimizes $\mathcal{L}_k^{(t)}$ (at final values of ν and μ) subject to nonnegativity constraints. Our update direction for \mathbf{p}_k is then given by $\mathbf{s}_k^{(t)} = \mathbf{p}_{\mathcal{L}_k}^{(t)} - \mathbf{p}_k^{(t)}$. We conduct a backtracking line search in direction $\mathbf{s}_k^{(t)}$ to find an update $\mathbf{p}_k^{(t+1)}$ that decreases $f_n(\mathbf{p}_k)$.

4 Inference for \mathbf{p} and β

We now address construction of confidence intervals and hypothesis tests. We focus on parameters β and \mathbf{p} , which we believe to be the most common targets for inference. To derive both marginal confidence intervals and more complex hypothesis tests, we consider a general setting in which we observe some estimate $\hat{\phi} = \phi(\mathbb{P}_n)$ of population quantity $\phi = \phi(P)$, where \mathbb{P}_n is the empirical distribution corresponding to a sample $\left\{ \left(\mathbf{W}_i, \mathbf{Z}_i, \mathbf{X}_i, \tilde{\mathbf{Z}}_i \right) \right\}_{i=1}^n$, P is its population analogue, and ϕ is a Hadamard directionally differentiable map into the parameter space Θ or into \mathbb{R} . To derive marginal confidence intervals for \mathbf{p} and β , we let $\phi(\mathbb{P}_n) = \hat{\theta}_n$ with $\phi(P) = \theta_0$. For hypothesis

tests involving multiple parameters, we specify $\phi(\mathbb{P}_n)$ as $2 [\sup_{\boldsymbol{\theta} \in \Theta} M_n(\boldsymbol{\theta}) - \sup_{\boldsymbol{\theta} \in \Theta_0} M_n(\boldsymbol{\theta})]$ with population analogue $\phi(P) = 0$ under $H_0 : \boldsymbol{\theta} \in \Theta_0$. In each case, we estimate the asymptotic distribution of $a(n) (\phi(\mathbb{P}_n) - \phi(P))$ for an appropriately chosen $a(n) \rightarrow \infty$.

As our model includes parameters that may lie on the boundary of the parameter space, the limiting distributions of our estimators and test statistics in general do not have a simple distributional form (Geyer, 1994), and the multinomial bootstrap will fail to produce asymptotically valid inference (Andrews, 2000). To address this, we employ a Bayesian subsampled bootstrap (Ishwaran et al., 2009), which consistently estimates the asymptotic distribution of our estimators when the true parameter is on the boundary. Let \mathbb{P}_n^ξ be a weighted empirical distribution $\sum_{i=1}^n \xi_{i,n} \mathbf{1}_{\mathbf{w}_i}$ with weights $\boldsymbol{\xi} \sim G$ for $G \sim \text{Dirichlet}(\frac{m}{n} \mathbf{1}_n)$. Then the bootstrap estimator $a(m) (\phi(\mathbb{P}_n^\xi) - \phi(\mathbb{P}_n))$ converges weakly to the limiting distribution of $a(n) (\phi(\mathbb{P}_n) - \phi(P))$ if we choose $m = m(n)$ such that $\lim_{n \rightarrow \infty} m = \infty$ and $\lim_{n \rightarrow \infty} \frac{m}{n} = 0$ (Ishwaran et al., 2009). We explore finite-sample behavior of the proposed bootstrap estimators with $m = \sqrt{n}$ in Section 6, finding good Type 1 error control.

To derive marginal confidence intervals for elements of $\boldsymbol{\theta}$, we let $a(n) = \sqrt{n}$ and $\phi(P) = \boldsymbol{\theta}(P)$. Then $\sqrt{m}(\hat{\boldsymbol{\theta}}_n^\xi - \hat{\boldsymbol{\theta}}_n)$ has the same limiting distribution as $\sqrt{n}(\hat{\boldsymbol{\theta}} - \boldsymbol{\theta})$. Therefore, for \hat{L}_c^q the c -th bootstrap quantile of the q -th element of $\sqrt{m}(\hat{\boldsymbol{\theta}}_n^\xi - \hat{\boldsymbol{\theta}}_n)$ and $\hat{\theta}_q$ the q -th element of the maximum (weighted) likelihood estimate $\hat{\boldsymbol{\theta}}$, an asymptotically $100(1 - \alpha)\%$ marginal confidence interval for θ_q is given by $(\hat{\theta}_q - \frac{1}{\sqrt{n}} \hat{L}_{1-\alpha/2}^q, \hat{\theta}_q - \frac{1}{\sqrt{n}} \hat{L}_{\alpha/2}^q)$.

As it may be of interest to test hypotheses about multiple parameters while leaving other parameters unrestricted (e.g., $\boldsymbol{\beta} = \mathbf{0}$ with unrestricted elements of \mathbf{p}), we also develop a procedure to test hypotheses of the form $H_0 : \{\theta_k = c_k : k \in \mathcal{K}_0\}$ for a set of parameter indices \mathcal{K}_0 against alternatives with $\boldsymbol{\theta}$ unrestricted. Letting Θ_0 indicate the parameter space under H_0 and Θ indicate the full parameter space, we conduct tests using test statistic $T_n := nT(\mathbb{P}_n) := 2n[\sup_{\boldsymbol{\theta} \in \Theta} M_n(\boldsymbol{\theta}) - \sup_{\boldsymbol{\theta} \in \Theta_0} M_n(\boldsymbol{\theta})]$. As noted above, T_n is in general not asymptotically χ^2 if (unknown) elements of \mathbf{p} or $\tilde{\mathbf{p}}$ lie at the boundary, and so we instead approximate the null distribution of T_n by bootstrap resampling from an empirical distribution projected onto an approximate null; this is closely related to the approach suggested by Hinkley (1988). Let $\hat{\mu}_{ij}$ denote $\exp(-\gamma_i)$ times the expectation of W_{ij} under the full model; $\hat{\mu}_{ij}^0$ denote the analogous quantity under H_0 ; and define $W_{ij}^0 = W_{ij} \frac{\hat{\mu}_{ij}^0}{\hat{\mu}_{ij}}$ if $\hat{\mu}_{ij} > 0$ and otherwise set $W_{ij}^0 = W_{ij} = 0$. In practice, we do not know $\hat{\mu}_{ij}$ or $\hat{\mu}_{ij}^0$, so we replace

W_{ij}^0 with $\hat{W}_{ij}^0 = \frac{\hat{\mu}_{ij}^0}{\hat{\mu}_{ij}}$, where $\hat{\mu}_{ij}$ and $\hat{\mu}_{ij}^0$ are, up to proportionality constant $\exp(\hat{\gamma}_i)$, fitted means for W_{ij} under the full and null models. After constructing $\hat{\mathbf{W}}^0$, we rescale its rows so row sums of $\hat{\mathbf{W}}^0$ and \mathbf{W} are equal. We then approximate the null distribution of T via bootstrap draws from $mT(\mathbb{P}_{0n}^\xi)$ where \mathbb{P}_{0n}^ξ is the Bayesian subsampled bootstrap distribution on $\hat{\mathbf{W}}_n^0$. We reject H_0 at level α if the observed likelihood ratio test statistic is larger than the $1 - \alpha$ quantile of the bootstrap estimate of its null distribution, or equivalently, if $T_n \geq \tilde{L}_{1-\alpha}^m$ for $\tilde{L}_{1-\alpha}^m$ the $1 - \alpha$ quantile of $mT(\mathbb{P}_{0n}^\xi)$.

5 Data Examples

5.1 Comparing detection effects across experiments

We now demonstrate the utility of our model in comparing different experimental protocols for high-throughput sequencing of microbial communities. We consider data generated in the Phase 2 experiment of Costea et al. (2017) (see also McLaren et al. (2019)), wherein ten human fecal specimens (labeled 1, 2, ..., 8, A and B) were mixed with a synthetic community of 10 taxa and prepared for shotgun metagenomic sequencing according to three different sample preparations (labeled H, Q, and W; samples A and B were only analyzed with preparation Q). The synthetic community was also sequenced alone. Raw sequencing data was processed into taxon abundance data using MetaPhlan2 (Truong et al., 2015) by McLaren et al. (2019). In addition to sequencing data, taxon abundances in the synthetic community were also measured using flow cytometry. We treat both sequencing and flow cytometry measurements as outcomes \mathbf{W} . We are interested in comparing the detection of taxa in the synthetic community across protocols H, Q and W relative to flow cytometry. We are specifically interested in testing the null hypothesis that all sequencing protocols share the same detection effects. To accomplish this, we estimate the 3×10 matrix $\boldsymbol{\beta}$ (we set $\boldsymbol{\beta}_{\cdot 10} = \mathbf{0}_3$ to ensure identifiability). Each row of $\boldsymbol{\beta}$ corresponds to a sequencing protocol, and each column corresponds to a taxon. For details regarding the specification of \mathbf{X} and other model parameters, see SI Section 4.1. Under our model, $\exp(\beta_{1j})$, $\exp(\beta_{1j} + \beta_{2j})$, and $\exp(\beta_{1j} + \beta_{3j})$ give the degree of over- or under-detection of taxon j relative to taxon 10 under protocols H, Q, and W,

respectively. We compare this model to a submodel in which $\beta_{kj} = 0$ for $k = 2, 3$ and all j . Under this null hypothesis, taxon detections relative to flow cytometry do not differ across protocols.

To compare predictive performance of these models, we perform 10-fold cross-validation on each model (see SI Section 4 for details). We use a bootstrapped likelihood ratio test to formally test our full model against the null submodel. We use the Bayesian subsampled bootstrap with $m = \sqrt{n}$ to illustrate its applicability, however, a multinomial bootstrap would also be appropriate as all parameters are in the interior of the parameter space in this case. In addition, we report point estimates and bootstrapped marginal 95% confidence intervals for detection effects estimated for each protocol under the full model. We also compare our results to MetaPhlAn2’s “plug-in” estimate of each sample’s composition.

Figure 1 summarizes 10-fold cross-validated estimated relative abundances from the full model, null model and plug-in estimates. We observe substantially better model fit for the full model (top row) than for the null model (middle row). At each flow cytometric relative abundance, cross-validated estimates from the full model are generally centered around the line $y = x$ (dotted line), whereas estimates from the null model exhibit substantial bias for some taxa. A bootstrapped likelihood ratio test of the null model (i.e., $H_0 : \beta_2 = \beta_3 = \mathbf{0}$) against the full model reflects this, and we reject the null with $p < 0.001$. Both the full and null models outperform the plug-in estimates of sample composition (bottom row), which produces substantially biased estimates of relative abundance relative to a flow cytometry standard. We report point estimates and marginal 95% confidence intervals for β in SI Section 4.3.

Using the full model, we estimate relative abundances with substantially greater precision under protocol W (top right) than under either other protocol (top left and center). This appears to be primarily due to lower variability in measurements taken via protocol W (bottom row). Our finding of greater precision of protocol W contrasts with Costea et al. (2017), who recommend protocol Q as a “potential benchmark for new methods” on the basis of median absolute error of centered-log-ratio-transformed plug-in estimates of relative abundance against flow cytometry measurements (as well as on the basis of cross-laboratory measurement reproducibility, which we do not examine here). The recommendations of Costea et al. (2017) are driven by performance of plug-in estimators subject to considerable bias, whereas we are able to model and remove a large degree of bias and

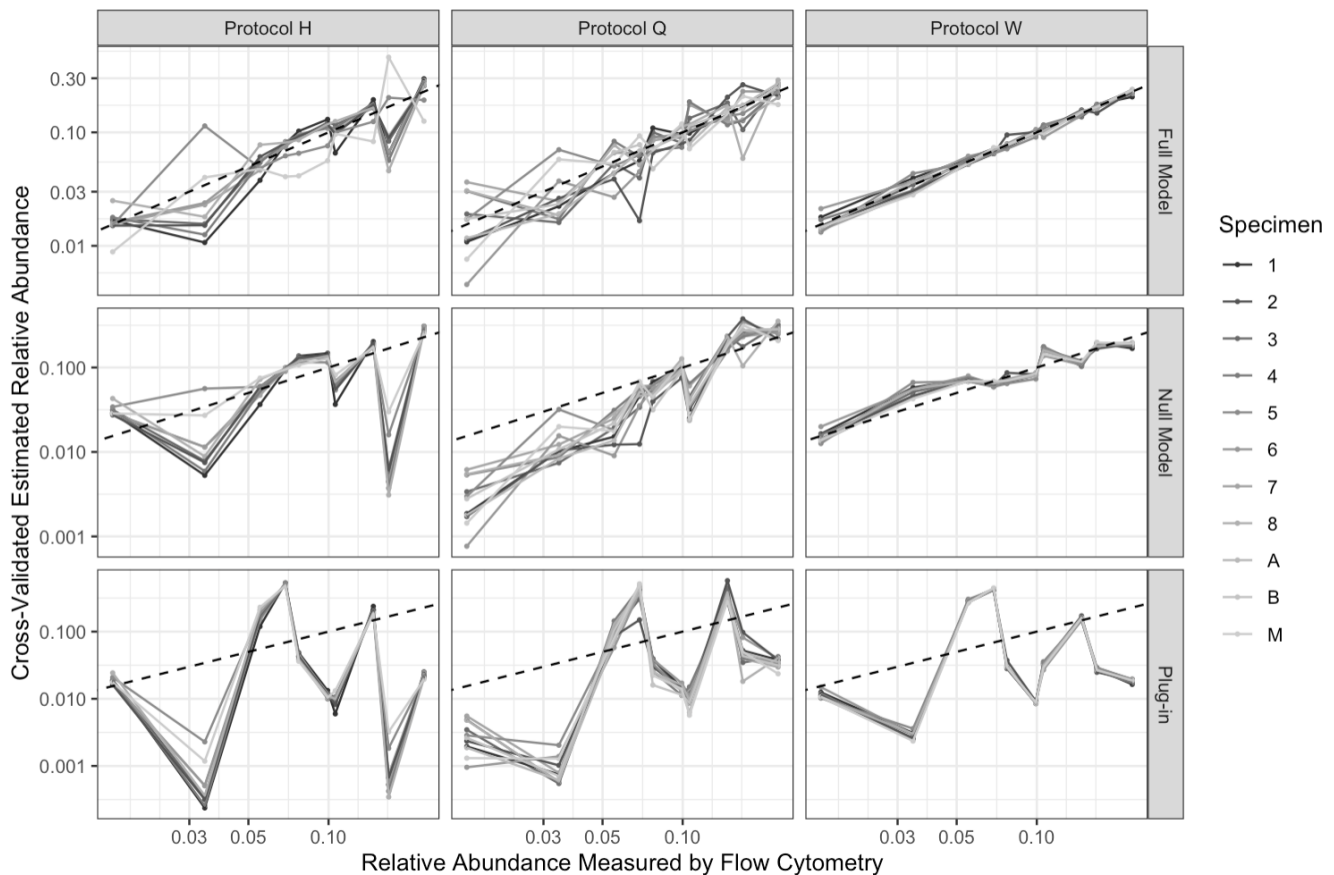


Figure 1: 10-fold cross-validated estimates of relative abundance (y-axis) in Costea et al. (2017) samples that were measured by whole-genome sequencing as well as plug-in estimates of relative abundance (bottom row). On the x-axis are relative abundance estimates obtained via flow cytometry (mean concentration in each taxon divided by sum across taxa). The top row contains estimates produced by a model containing separate detection effects β for each protocol; the middle row contains output from a model assuming a single common detection effect across protocols; and the bottom row contains “plug-in” estimates from MetaPhlAn2 output. Results for each protocols H, Q, and W are given in the leftmost, center, and rightmost columns, respectively. Within each pane, estimated relative abundances for the same sample are connected by line segments, and the line $y = x$ is indicated with a dotted line.

can hence focus on residual variation after bias correction. We also note that Costea et al. (2017) did not use MetaPhlan2 to construct abundance estimates, which may partly account our different conclusions.

5.2 Estimating contamination via dilution series

We next illustrate how to use our model to estimate and remove contamination in samples. We consider data from Karstens et al. (2019), who generated 9 samples via three-fold dilutions of a synthetic community containing 8 distinct strains of bacteria which each account for 12.5% of the DNA in the community. Despite only 8 strains being present in the synthetic community, 248 total strains were identified based on sequencing (see SI Section 5.1 for data processing details). We refer to the 8 strains in the synthetic community as “target” taxa and other strains as “off-target.” Note that Karstens et al. (2019) identified one strain as a likely mutant of synthetic community member *S. enterica*, and we refer to this strain as *S. [unclassified]*.

To evaluate the performance of our model, we perform three-fold cross-validation and estimate relative abundance in the hold-out fold. We consider $\mathbf{p} \in \mathbb{R}^{2 \times 248}$, where the first row contains the known composition of the training fold ($\mathbf{0}_{240}^T \frac{1}{8} \mathbf{1}_8^T$) and the second row is unknown and the target of inference (see SI Section 5.2 for full model specification). We evenly balance dilutions across folds, and using our proposed reweighted estimator to fit a model that accounts for the serial dilutions. We set $\tilde{K} = 1$ and let $\tilde{\mathbf{Z}}_i = \exp(\gamma_i) \times 3^{d_i}$, where d_i is the number of three-fold dilutions sample i has undergone. This model reflects the assumption that the ratio of expected contaminant reads to expected non-contaminant reads is proportional to 3^{d_i} . To avoid improperly sharing information about contamination amounts across folds, we further parametrize $\tilde{\mathbf{Z}}$ in terms of a fixed, unknown parameter $\tilde{\alpha} \in \mathbb{R}$ by multiplying each row of $\tilde{\mathbf{Z}}$ corresponding to a held-out sample by $\exp(\tilde{\alpha})$. This preserves information about relative dilution within the held-out fold without treating samples in the training and held-out folds as part of the same dilution series. We model a single differential detection effect β_j for each of the 8 taxa in the synthetic community, setting $\beta_J = 0$ for the reference taxon *L. fermentum* for identifiability. Because β_j is not identifiable for off-target taxa, we also fix $\beta_j = 0$ for $j = 1, \dots, 240$.

Figure 2 shows data from Karstens et al. (2019) along with summaries of our analysis. Our

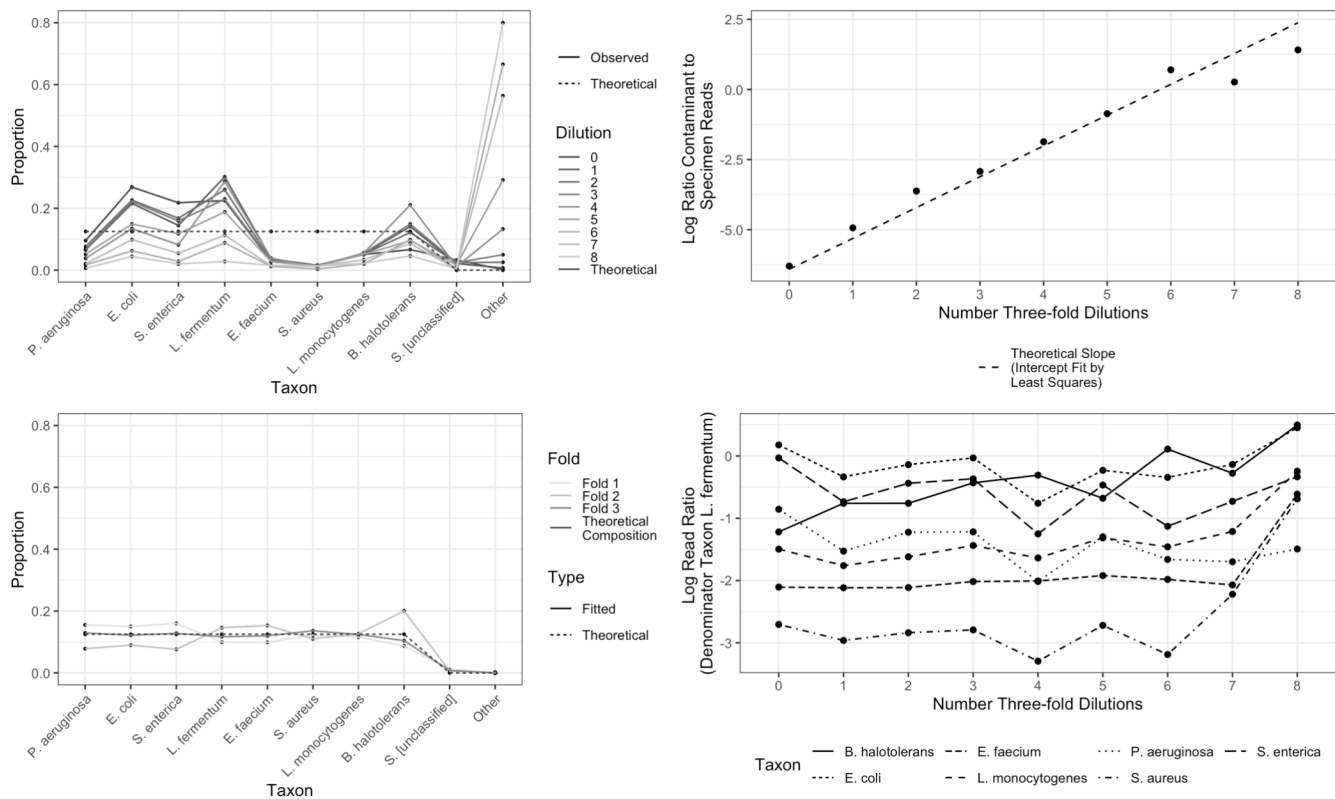


Figure 2: Data from Karstens et al. (2019), and estimates and summaries from the fitted model. (Top left) Observed read proportions by taxon and dilution, with theoretical synthetic composition indicated by dotted line. (Top right) The log-ratio of total contaminant reads to total non-contaminant reads (excluding *S. [unclassified]*). The dotted line has slope $\log(3)$, with intercept fit via least squares. (Bottom left) Fitted read proportions obtained from each cross-validation fold, with theoretical synthetic composition indicated by dotted line. Every fold produces abundance estimates that improve over observed read proportions. (Bottom right) The log-ratio of reads for target taxa to reference taxon *L. fermentum* is relatively constant across increasing numbers of dilutions.

estimate for the relative abundance of taxa in samples in the held-out fold \mathbf{p}_2 . improves on the performance of plug-in estimators (Figure 2, left panels) by taking into account two forms of structure in the Karstens et al. (2019) data. First, in each successive three-fold dilution, we observe approximately three times more contamination relative to the number of non-contaminant reads (Figure 2, top right). In addition, our model accounts for the degree of under- (or over-) detection of target taxa relative to *L. fermentum*. We observe that taxon detection is reasonably constant across dilutions (Figure 2, bottom right). However, we do observe greater variability in taxon detections at higher dilutions, most likely because we observe comparatively few reads ($\sum_{j=1}^{248} W_{\{i:d_i=1\}j} \approx 227,000$ while $\sum_{j=1}^{248} W_{\{i:d_i=8\}j} \approx 8,000$).

In terms of root mean squared error (RMSE) $\sqrt{1/J \sum_{j=1}^J (\hat{p}_j - p_j)^2}$, our cross-validated estimates (0.0037, 0.0073, and 0.0033) substantially outperform the “plug-in” estimates given by sample read proportions in any of these dilutions (median 0.017; range 0.013 – 0.022). This is not an artifact of incorporating information from 3 samples in each cross-validation fold, as pooling reads across all samples yields an estimator with RMSE 0.014.

Fitting a model to this relatively small dataset and evaluating its performance using cross validation prohibits the reasonable construction of confidence intervals. Therefore, to evaluate the performance of our proposed approach to generating confidence intervals, we also fit a model which treats all samples as originating from a single specimen of unknown composition. β is not identifiable in this setting, so we set it equal to zero and do not estimate it. We set $\tilde{K} = 1$ and $\tilde{\mathbf{Z}}_i = \exp(\gamma_i) \times 3^{d_i}$ as before (the need for $\tilde{\alpha}$ is alleviated). Strikingly, under this model, marginal 95% confidence intervals for elements of \mathbf{p} included zero for 238 out of 240 off-target taxa (empirical coverage of 99.2% when true $p_{kj} = 0$). No interval estimates for target taxa included zero. This suggests that applying our proposed approach to data from a dilution series experiment can aid in evaluating whether taxa detected by next-generation sequencing are actually present in a given specimen.

6 Simulations

6.1 Sample size and predictive performance

To evaluate the predictive performance of our model on microbiome datasets of varying size, we use data from 65 unique specimens consisting of synthetic communities of 1, 2, 3, 4, or 7 species combined in equal abundances. Brooks et al. (2015) performed 16S amplicon sequencing on 80 samples of these 65 specimens across two plates of 40 samples each. Very few reads in this dataset were ascribed to taxa outside the 7 present by design, so we limit analysis to these taxa. To explore how prediction error varies with number of samples of known composition, we fit models treating randomly selected subsets of $n_{\text{known}} \in \{3, 5, 10, 20\}$ samples per plate as known. In each model, we included one source of unknown contamination for each plate and estimate a detection vector $\beta \in \mathbb{R}^J$. For each n_{known} , we drew 100 independent sets of samples to be treated as known, requiring that each set satisfy an identifiability condition in β (see SI Section 6.1). On each set, we fit both the unweighted and reweighted models, treating n_{known} samples as having known composition and $80 - n_{\text{known}}$ samples as arising from unique specimens of unknown composition.

We observe similar RMSE for the reweighted and unweighted estimators. For n_{known} equal to 3, 5, 10, and 20, we observe RMSE 0.041, 0.037, 0.035, and 0.032 (to 2 decimal places) for both estimators. By comparison, the RMSE for the plugin estimator $\frac{W_{ij}}{\sum_{j=1}^J W_{ij}}$ is 0.173. Notably, RMSE decreases but does not approach zero as larger number of samples are treated as known, which reflects that we estimated each relative abundance profile on the basis of a single sample.

With respect to correctly estimating p_{kj} when $p_{kj} = 0$, we again see very similar performance of the reweighted and unweighted Poisson estimators. Out of 100 sets, unweighted estimation yields $\hat{p}_{kj} = 0$ for 53%, 55%, 59%, and 64% of $\{k, j\}$ pairs for which $p_{kj} = 0$ (n_{known} equal to 3, 5, 10, and 20). The corresponding figures for the reweighted estimator are 53%, 55%, 58%, and 63%. The plug-in estimator sets 51% of these relative abundances equal to zero. While we observe the proportion of theoretical zero relative abundances estimated to be zero increases in number of samples treated as known regardless of estimator, in general we do not expect this proportion to approach 1 as number of known samples increases. We also note that our model is not designed

to produce prediction intervals, and confidence intervals for a parameter estimated from a single observation are unlikely to have reasonable coverage. Finally, we acknowledge that despite the excellent performance of our model on the data of Brooks et al. (2015), our model does not fully capture sample cross-contamination known as index-hopping (Hornung et al., 2019), which likely affects this data.

6.2 Type 1 error rate and power

To investigate the Type 1 error rate and power of tests based on reweighted and unweighted estimators, we simulate data arising from a set of hypothetical dilution series. In each simulated dataset, we observe reads from dilution series of four specimens: two specimens of known composition and two specimens of unknown composition (specimens A and B). Each dilution series consists of four samples: an undiluted sample from a specimen as well as a 9-, 81-, and 729-fold dilution of the specimen. We vary the number of taxa $J \in \{5, 20\}$, as well as the magnitude of elements of β , the number of samples, and the distribution of $W_{ij}|\mu_{ij}$.

We consider three different values of $\beta \in \mathbb{R}^J$: $\beta = 0\beta^*$, $\beta = \frac{1}{10}\beta^*$, and $\beta = \beta^*$ where $\beta^* = \begin{pmatrix} 3 & -1 & 1 & -3 & 0 \end{pmatrix}$ when $J = 5$ and $\beta^* = \begin{pmatrix} 3 & -1 & 1 & -3 & 3 & -1 & \dots & -3 & 0 \end{pmatrix}$ when $J = 20$. We base the magnitude of entries of β^* using the observed magnitude of entries of $\hat{\beta}$ in our analysis of Costea et al. (2017) data. We vary the number of samples between either a single dilution series from each specimen or three dilution series from each specimen (for a total of nine samples per specimen). We draw $W_{ij}|\mu_{ij}$ from either a Poisson(μ_{ij}) distribution or a Negative Binomial distribution with mean parameter μ_{ij} and size parameter $s = 13$. $s = 13$ was chosen to approximate the Karstens et al. (2019) data via a linear regression of fitted mean-centered squared residuals. In all settings we simulate $\{\gamma_i\}_{i=1}^n$ from a log-normal distribution with parameters $\mu = \min(13.5 - 1.5d_i, 12)$ and $\sigma^2 = 0.05$. These values were chosen based on observed trends in reads from target taxa in the data of Karstens et al. (2019) data. In all settings, the first specimen has true relative abundance proportional to $(1, 2^{\frac{4}{J-1}}, 2^{2 \cdot \frac{4}{J-1}}, \dots, 2^4)$, that is, taxon J is 16 times more abundant than taxon 1. The second specimen has true relative abundance proportional to $(2^4, \dots, 2^{\frac{4}{J-1}}, 1)$. When $J = 5$, the first two taxa are absent from specimen A, and when $J = 20$, first eight taxa are absent from specimen A. Relative abundances in the remaining taxa form

an increasing power series such that the first taxon present in nonzero abundance has relative abundance that is 1/100-th of the relative abundance of taxon J . The relative abundance profile of specimen B is given by the relative abundance vector for specimen A in reverse order. We also simulate the degree of contamination as scaling with dilution. When comparing samples with the same read depth, on average a 9-fold diluted sample will contain 9 times more contaminant reads than an undiluted sample (see Section 5.2 and Figure 2, top right). We simulate contamination from a source containing equal relative abundance of all taxa. We set $\tilde{\mathbf{Z}} \in \mathbb{R}^n$ such that $\tilde{Z}_i = 9^{d_i}$ where d_i is the degree of dilutions of sample i , and $\tilde{\gamma} = -3.7$, as we observe in Karstens et al. (2019) data.

Figure 3 summarizes our simulation results. Empirical performance of bootstrapped likelihood ratio tests of $H_0 : \boldsymbol{\beta} = 0$ against $H_A : \boldsymbol{\beta} \neq 0$ reveals good performance, even for small sample sizes. Unsurprisingly, we observe improved Type 1 error control and power at larger sample sizes. Tests based on the reweighted estimator generally improved Type 1 error compared to the unweighted estimator, with the greatest improvements observed for data simulated from a negative binomial distribution (mean Type 1 error across simulations was 0.15 for the unweighted estimator and 0.04 for the reweighted estimator). Surprisingly, Type 1 error control appears to improve when the number of taxa J is larger (mean Type 1 error was 0.11 for $J = 5$ and 0.05 for $J = 10$). This may in part be a result of simulating W_{ij} as conditionally independent given covariates, γ_i , and other parameters, and we conjecture that simulating under a conditional dependence structure might yield different results. Power to reject the null hypothesis is very high when the data generating process is Poisson, as well as for strong alternatives ($\boldsymbol{\beta} = \boldsymbol{\beta}^*$) when the data follows a negative binomial distribution.

7 Discussion

In this paper, we introduce a statistical method to model measurement error due to contamination and differential detection of taxa in microbiome experiments. Our method builds on previous work in several ways. By directly modeling the output of microbiome experiments, we do not rely on data transformations that discard information regarding measurement precision, such as

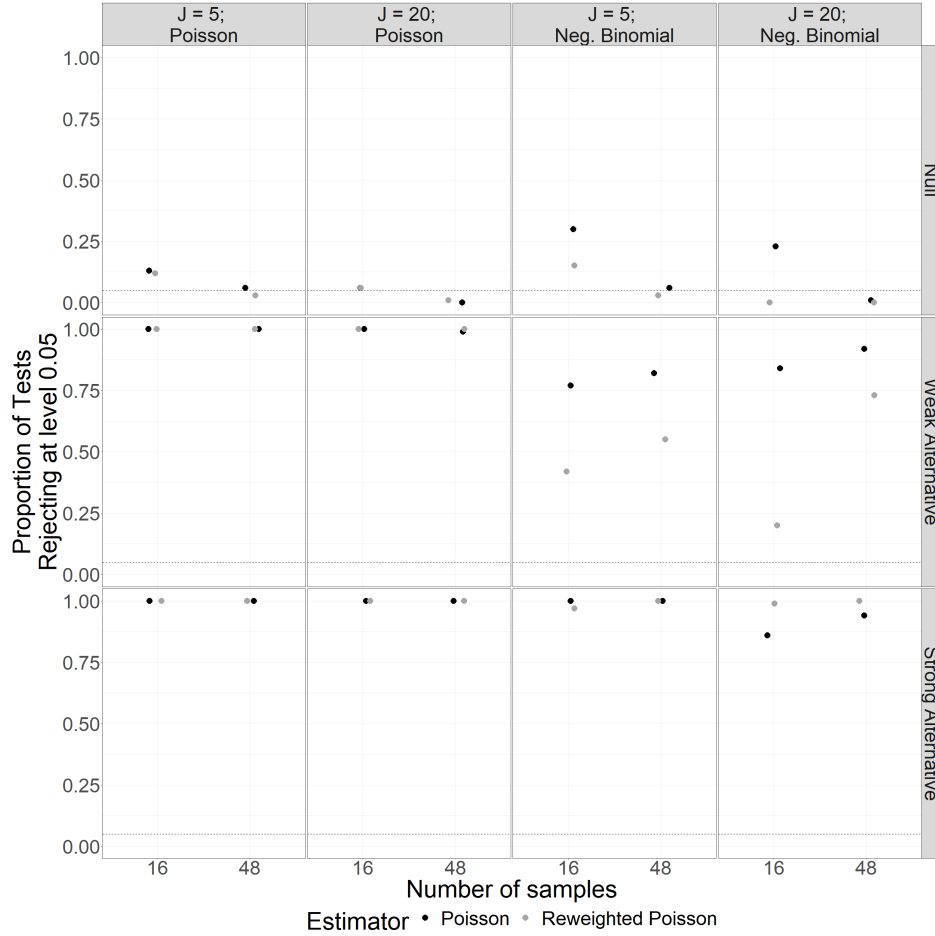


Figure 3: The Type 1 error (top row) and power of our proposed likelihood ratio tests for both the unweighted and reweighted estimators. For each combination of sample size, number of taxa, and conditional distribution of data, we show the results of 100 bootstrap samples. Performance of tests of $H_0 : \boldsymbol{\beta} = 0$ against a general alternative are summarized in terms of empirical rejection rates at level $\alpha = 0.05$ (y-axis), with sample size plotted on the x-axis. Columns give the conditional distribution of data (Poisson or Negative Binomial) and number of taxa J . Rows specify whether data was simulated under the null $\boldsymbol{\beta} = 0$, under a “weak” alternative with $\boldsymbol{\beta} = \frac{1}{10}\boldsymbol{\beta}^*$ (i.e., $\boldsymbol{\beta} \neq 0$ of small magnitude), or under a “strong” alternative $\boldsymbol{\beta} = \boldsymbol{\beta}^*$ (i.e., $\boldsymbol{\beta} \neq 0$ of larger magnitude).

ratio- or proportion-based transformations. This affords our method the key advantage of estimating relative abundances lying on the boundary of the simplex, which is typically precluded by transformation-based approaches. Accordingly, we implement inference tools appropriate to the non-standard parameter space that we consider. The advantage of estimating relative abundances on the boundary of the simplex is not purely theoretical, and we show that our interval estimates do indeed include boundary values, and demonstrate above-nominal empirical coverage in an analysis of data from Karstens et al. (2019). Furthermore, our reweighting estimator allows for flexible mean-variance relationships without the need to specify a parametric model. Our approach to parameter estimation does not assume that observations are counts, and therefore our method can be applied to a wide array of microbiome data types, including proportions, coverages and cell concentrations as well as counts. Finally, our method can accommodate complex experimental designs, including analysis of mixtures of samples, technical replicates, dilution series, detection effects that vary by experimental protocol or specimen type, and contamination impacting multiple samples. Contamination is commonly addressed via “pre-processing” data, thereby conditioning on the decontamination step. In contrast, by simultaneously estimating contamination along with all other model parameters, holistic uncertainty in estimation is captured by our approach.

Another advantage of our methodology is that we do not require the true composition of any specimens to be known. For example, our test of equal detection effects across protocols in Costea et al. (2017) can be performed without knowledge of specimen composition. Accordingly, our approach provides a framework for comparing experimental protocols in the absence of synthetic communities, which can be challenging to construct.

In addition, we expect that our method may have substantial utility applied to dilution series experiments, as illustrated in our analysis of data from Karstens et al. (2019). Dilution series are relatively low-cost and scalable (especially in comparison to synthetic communities) and may be especially advantageous when the impact of sample contamination on relative abundance estimates is of particular concern. With this said, we strongly recommend against testing the composite null $H_0 : p_{kj} > 0$ against the point alternative $H_A : p_{kj} = 0$, as these hypotheses are statistically indistinguishable on the basis of any finite sample of reads. However, we are able to determine the degree to which our observations are consistent with the *absence* of any given taxon, and therefore

we can meaningfully test $H_0 : p_{kj} = 0$ against a general alternative.

We provide a number of suggestions for future research. Firstly, we have not formally identified conditions that ensure the identifiability of parameters of our model. In some situations it is trivial to diagnose non-identifiability through examination of design matrices \mathbf{Z} , \mathbf{X} and $\tilde{\mathbf{Z}}$ alongside known entries of \mathbf{p} and $\boldsymbol{\beta}$. In complex situations, this is not straightforward. We defer investigation of these conditions to future work. For now, we note that the parameter estimation algorithm we propose is stable for identifiable means and challenges in model-fitting may betray non-identifiability.

The focus of our paper was on \mathbf{p} and $\boldsymbol{\beta}$ as targets of inference. Future research could investigate extensions to our model that connect relative abundances \mathbf{p} to covariates of interest, allowing the comparison of average relative abundances across groups defined by covariates, for example. Our proposed bootstrap procedures may also aid the propagation of uncertainty to group-level comparisons of relative abundances in downstream analyses.

In addition, while we focus applications of our model on microbiome data, our model could be applied to a broad variety of data structures obtained from high-throughput sequencing, such as single-cell RNAseq. We leave these applications to future work.

Software implementing the methodology described in this paper are implemented in a R package available at <https://github.com/statdivlab/tinyvamp>. Code to reproduce all simulations and data analyses are available at https://github.com/statdivlab/tinyvamp_supplementary.

References

- Andrews, D.W. (2000). Inconsistency of the bootstrap when a parameter is on the boundary of the parameter space. *Econometrica*, 399–405.
- Bazaraa, M.S. (2006). Nonlinear programming: theory and algorithms.
- Brooks, J.P. et al (2015). The truth about metagenomics: quantifying and counteracting bias in 16s rna studies. *BMC Microbiology* 15(1), 1–14.
- Callahan, B.J. et al (2016). DADA2: high-resolution sample inference from illumina amplicon data. *Nature Methods* 13(7), 581.

- Clausen, D.S. and Willis, A.D. (2021). Evaluating replicability in microbiome data. *Biostatistics*.
- Costea, P.I. et al (2017). Towards standards for human fecal sample processing in metagenomic studies. *Nature Biotechnology* 35(11), 1069.
- Dai, Z. et al (2019). Batch effects correction for microbiome data with dirichlet-multinomial regression. *Bioinformatics* 35(5), 807–814.
- Davis, N.M. et al (2018). Simple statistical identification and removal of contaminant sequences in marker-gene and metagenomics data. *Microbiome* 6(1), 1–14.
- Gagnon-Bartsch, J.A. and Speed, T.P. (2012). Using control genes to correct for unwanted variation in microarray data. *Biostatistics* 13(3), 539–552.
- Geyer, C.J. (1994). On the asymptotics of constrained m-estimation. *The Annals of statistics*, 1993–2010.
- Gibbons, S.M., Duvallet, C. and Alm, E.J. (2018). Correcting for batch effects in case-control microbiome studies. *PLOS Computational Biology* 14(4), e1006102.
- Hinkley, D.V. (1988). Bootstrap methods. *Journal of the Royal Statistical Society: Series B (Methodological)* 50(3), 321–337.
- Hornung, B.V., Zwiittink, R.D. and Kuijper, E.J. (2019). Issues and current standards of controls in microbiome research. *FEMS microbiology ecology* 95(5), fiz045.
- Ishwaran, H., James, L.F. and Zarepour, M. (2009). An alternative to the m out of n bootstrap. *Journal of Statistical Planning and Inference* 139(3), 788–801.
- Johnson, W.E., Li, C. and Rabinovic, A. (2007). Adjusting batch effects in microarray expression data using empirical bayes methods. *Biostatistics* 8(1), 118–127.
- Karstens, L. et al (2019). Controlling for contaminants in low-biomass 16s rrna gene sequencing experiments. *MSystems* 4(4), e00290–19.

- Knights, D. et al (2011). Bayesian community-wide culture-independent microbial source tracking. *Nature methods* 8(9), 761–763.
- Leek, J.T. and Storey, J.D. (2007). Capturing heterogeneity in gene expression studies by surrogate variable analysis. *PLoS genetics* 3(9), e161.
- McCullagh, P. (1983). Quasi-likelihood functions. *The Annals of Statistics* 11(1), 59–67.
- McLaren, M.R., Willis, A.D. and Callahan, B.J. (2019). Consistent and correctable bias in metagenomic sequencing experiments. *eLife* 8.
- Nearing, J.T., Comeau, A.M. and Langille, M.G. (2021). Identifying biases and their potential solutions in human microbiome studies. *Microbiome* 9(1), 1–22.
- Oron, A.P. and Flournoy, N. (2017). Centered isotonic regression: point and interval estimation for dose–response studies. *Statistics in Biopharmaceutical Research* 9(3), 258–267.
- Pollock, J. et al (2018). The madness of microbiome: attempting to find consensus “best practice” for 16S microbiome studies. *Appl. Environ. Microbiol.* 84(7), e02627–17.
- Quast, C. et al (2012). The silva ribosomal rna gene database project: improved data processing and web-based tools. *Nucleic acids research* 41(D1), D590–D596.
- Römisch, W. (2004). Delta method, infinite dimensional.
- Salter, S.J. et al (2014). Reagent and laboratory contamination can critically impact sequence-based microbiome analyses. *BMC biology* 12(1), 1–12.
- Shenhav, L. et al (2019). Feast: fast expectation-maximization for microbial source tracking. *Nature Methods* 16(7), 627–632.
- Silverman, J.D. et al (2021). Measuring and mitigating pcr bias in microbiota datasets. *PLoS computational biology* 17(7), e1009113.

- Sims, A.H. et al (2008). The removal of multiplicative, systematic bias allows integration of breast cancer gene expression datasets—improving meta-analysis and prediction of prognosis. *BMC medical genomics* 1(1), 1–14.
- Sinha, R. et al (2017). Assessment of variation in microbial community amplicon sequencing by the Microbiome Quality Control (MBQC) project consortium. *Nature Biotechnology* 486(11), 207.
- Truong, D.T. et al (2015). Metaphlan2 for enhanced metagenomic taxonomic profiling. *Nature methods* 12(10), 902–903.
- Weiss, S. et al (2014). Tracking down the sources of experimental contamination in microbiome studies. *Genome biology* 15(12), 1–3.
- Willner, D. et al (2012). Comparison of dna extraction methods for microbial community profiling with an application to pediatric bronchoalveolar lavage samples. *PloS one* 7(4), e34605.
- Zhao, N. and Satten, G.A. (2021). A log-linear model for inference on bias in microbiome studies. In *Statistical Analysis of Microbiome Data*, pp. 221–246. Springer.

SUPPLEMENTARY MATERIAL

8 Additional details for reweighted estimator

In Section 3, we introduced a weighted Poisson log-likelihood with weight for the likelihood contribution of W_{ij} given by

$$\hat{w}_{ij} = \frac{\hat{\mu}_{ij} + 1}{\hat{\sigma}_{ij}^2 + 1}$$

where $\hat{\mu}_{ij}$ is the fitted mean for W_{ij} given parameters $\hat{\theta}$ estimated under a Poisson likelihood and read depth $W_{i\cdot}$ arising from a model fit to \mathbf{W} via a Poisson likelihood (without reweighting) and $\hat{\sigma}_{ij}^2$ is a fitted value from a monotone regression of squared residuals $(W_{ij} - \hat{\mu}_{ij})^2$ on fitted means $\hat{\mu}_{ij}$ (with $i = 1, \dots, n$ and $j = 1, \dots, J$). In other words, $\hat{\sigma}_{ij}^2$ is an estimate of $\text{var}(W_{ij}|W_{i\cdot}, \theta)$.

To motivate why this reweighting is reasonable, we consider the case in which θ is in the interior of the parameter space Θ . In this setting we can express the Poisson MLE as a solution to the following score equations:

$$\left\{ \begin{array}{l} \sum_{i,j} \frac{1}{\mu_{ij}} \left[\frac{\partial}{\partial \theta_1} \mu_{ij} \right] (W_{ij} - \mu_{ij}) = 0 \\ \vdots \\ \sum_{i,j} \frac{1}{\mu_{ij}} \left[\frac{\partial}{\partial \theta_L} \mu_{ij} \right] (W_{ij} - \mu_{ij}) = 0 \end{array} \right.$$

Equivalently, we can write

$$\sum_{i,j} \frac{1}{\mu_{ij}} \mathbf{g}_{ij}(\theta) = 0$$

letting $\mathbf{g}_{ij} = \left[\frac{\partial}{\partial \theta^T} \mu_{ij} \right] (W_{ij} - \mu_{ij})$. Hence, we can view this system of equations as a weighted sum of zero expectation terms \mathbf{g}_{ij} with weights given by $\frac{1}{\mu_{ij}}$ — that is, one over a model-based estimate of $\text{Var}(W_{ij} - \mu_{ij})$. In this setting, if the Poisson mean-variance relationship holds and the score equations have a unique solution, we expect the estimator given by this solution to be asymptotically efficient (McCullagh, 1983), whereas when a different mean-variance relationship holds, in general we expect to lose efficiency. In contrast, when the Poisson mean-variance relationship does not hold, we expect to be able to improve efficiency by reweighting the score

equations with a more flexible estimator of $\text{Var}(W_{ij} - \mu_{ij})$. To accomplish this, we use a consistent estimator of θ , the Poisson MLE $\hat{\theta}$, to estimate $\boldsymbol{\mu}$ and $\text{Var}(W_{ij}|\mu_{ij})$. Specifically, we estimate $\sigma^2(\hat{\mu}_{ij}) := \text{Var}(W_{ij}|W_i, X_i, Z_i, \tilde{Z}_i, \boldsymbol{\beta}, \mathbf{p}, \tilde{\mathbf{p}}, \tilde{\boldsymbol{\gamma}})$ under the assumption that $\sigma^2(\cdot)$ is an increasing function via a centered isotonic regression of $(W_{ij} - \hat{\mu}_{ij})^2$ on $\hat{\mu}_{ij}$. Weighting the log-likelihood contribution of W_{ij} , $l_{ij} := W_{ij}\log(\mu_{ij}) - \mu_{ij}$, by a factor of $\frac{\hat{\mu}_{ij}}{\hat{\sigma}_{ij}^2}$ then yields reweighted score equations

$$\sum_{i,j} \frac{\hat{\mu}_{ij}}{\hat{\sigma}_{ij}^2} \frac{1}{\mu_{ij}} \mathbf{g}_{ij}(\theta) = \sum_{i,j} \frac{\hat{\mu}_{ij}}{\mu_{ij}} \frac{1}{\hat{\sigma}_{ij}^2} \mathbf{g}_{ij}(\theta)$$

in which each \mathbf{g}_{ij} is, up to a factor of $\frac{\hat{\mu}_{ij}}{\mu_{ij}} \xrightarrow{p} 1$, weighted by the inverse of a flexible estimate of $\text{Var}(W_{ij}|\mu_{ij})$. In practice, however, the weighting above may be unstable when $\hat{\mu}_{ij}$ and $\hat{\sigma}_{ij}^2$ are small. Hence, we weight instead by $\frac{\hat{\mu}_{ij}+1}{\hat{\sigma}_{ij}^2+1}$ to preserve behavior of weights when the estimated mean and variance are both large (where reweighting is typically most important) and stabilizes them when these quantities are small.

9 Supporting theory for proposed model and estimators

Throughout this section, we will use the following notation:

- $\mathbf{W}_i = (W_{i1}, \dots, W_{iJ})$: a measured outcome of interest in sample i across taxa $j = 1, \dots, J$. We also use \mathbf{W} without subscript i where this does not lead to ambiguity
- \mathbf{X}_i here denotes covariates (Z_i, X_i, \tilde{Z}_i) described in the main text
- \mathcal{W} : the support of \mathbf{W}
- \mathcal{X} : the support of \mathbf{X}
- \mathcal{W} : the support of $W := \sum_{j=1}^J W_j$
- v : a weighting function from $\mathcal{W} \times \mathcal{X}$ into $\mathbf{R}_{>0}^J$. For simplicity of notation, we frequently suppress dependence on W_i and \mathbf{X}_i and write v_{ij} to indicate $v_j(W_i, \mathbf{X}_i)$
- \hat{v}_n : an empirical weighting function estimated from a sample of size n

- θ : unknown parameters $(\mathbf{p}, \boldsymbol{\beta}, \tilde{\mathbf{p}}, \tilde{\boldsymbol{\gamma}})$; we denote the true value with θ_0
- $\boldsymbol{\mu}_\theta$: a parametrization of the mean model given in equation (5) in main text; $\mathbb{E}[\mathbf{W}|\mathbf{X}, \gamma, \theta] = \exp(\gamma)\boldsymbol{\mu}_\theta(\mathbf{X})$; we typically suppress dependence on \mathbf{X}
- $M_n^v(\theta)$: profile log likelihood under weighting function v , evaluated at θ on a sample of size n
- $M^v(\theta)$: expected profile log likelihood under weighting function v , evaluated at θ

9.1 Assumptions

- (A) We draw triples $(\mathbf{W}, \mathbf{X}, \Gamma) \stackrel{\text{iid}}{\sim} P_{\theta_0}$ (of which we observe only (\mathbf{W}, \mathbf{X})) where \mathbf{W} has bounded support $\mathcal{W} \subset \mathbb{R}_{\geq 0}^J$, \mathbf{X} has bounded support $\mathcal{X} \subset \mathbb{R}^p$, Γ has bounded support $\mathcal{G} \subset \mathbb{R}$.
- (B) Letting θ denote $(\mathbf{p}, \boldsymbol{\beta}, \tilde{\mathbf{p}}, \tilde{\boldsymbol{\gamma}})$, for a set of known functions from \mathcal{X} to $\mathbb{R}_{\geq 0}^J$ $\{\boldsymbol{\mu}_\theta : \theta \in \Theta\}$ we have that $\mathbb{E}[\mathbf{W}|\Gamma, \mathbf{X}] = \exp(\Gamma)\boldsymbol{\mu}_{\theta_0}(\mathbf{X})$ and $\mathbb{E}[\mathbf{W}|\Gamma, \mathbf{X}, \mathbf{W}.] = \mathbf{W} \cdot \frac{\boldsymbol{\mu}_{\theta_0}(\mathbf{X})}{\boldsymbol{\mu}_{\theta_0}(\mathbf{X})}$, with $\mu_\theta(x)$ differentiable in θ for all $x \in \mathcal{X}$ and for each fixed $\theta \in \Theta$, $\mu_\theta(x)$ a bounded function on \mathcal{X} .
- (C) For almost all $\mathbf{x} \in \mathcal{X}$, $\gamma \in \mathcal{G}$, $P([\sum_{j=1}^J W_j] > \epsilon | \mathbf{X} = \mathbf{x}, \Gamma = \gamma) = 1$ for some $\epsilon > 0$.

9.2 Form of profile log likelihood

We first derive the form of a log likelihood in which Γ_i , treated as a fixed effect γ_i , has been profiled out and characterize its population analogue. Estimating Γ_i as a fixed effect via maximum likelihood under a Poisson likelihood for \mathbf{W} with (positive) weight v_{ij} given to the likelihood contribution of W_{ij} , we obtain the following profile log likelihood:

$$M_n^v(\theta) := \frac{1}{n} \sum_{i=1}^n \sup_{\gamma_i \in \mathbb{R}} \left[\sum_{j=1}^J v_{ij} \left(W_{ij} \log[\exp(\gamma_i)\mu_{\theta j}(X_i)] - \exp(\gamma_i)\mu_{\theta j}(X_i) \right) \right] \quad (12)$$

$$= \frac{1}{n} \sum_{i=1}^n \sum_{j=1}^J \left[v_{ij} \left(W_{ij} \log \left[\frac{\mathbf{v}_i \cdot \mathbf{W}_i}{\mathbf{v}_i \cdot \boldsymbol{\mu}_\theta} \mu_{\theta j} \right] - \frac{\mathbf{v}_i \cdot \mathbf{W}_i}{\mathbf{v}_i \cdot \boldsymbol{\mu}_\theta} \mu_{\theta j} \right) \right] \quad (13)$$

where we suppress dependence on \mathbf{X}_i for simplicity in the second row. We derive the profile likelihood in the second row via differentiation with respect to γ_i ; the optimum is unique by

convexity of $ay - b\exp(y)$ in y when $a, b > 0$. We use $\mathbf{v}_i \cdot \mathbf{W}_i$ to denote $\sum_{j=1}^J v_{ij} W_{ij}$ and similarly for $\mathbf{v}_i \cdot \boldsymbol{\mu}_\theta$.

We now allow weights $\mathbf{v}_i = (v_{i1}, \dots, v_{iJ})$ to be given as a (bounded positive) function of \mathbf{X}_i and $\mathbf{W}_i := \sum_{j=1}^J W_{ij}$ and examine the population analogue $M^v(\theta)$ of the weighted profile log likelihood $M_n^v(\theta)$.

$$M^v(\theta) = \mathbb{E}_{\mathbf{W}, \mathbf{X}, \Gamma} \left[\sum_{j=1}^J v_{ij} \left(W_{ij} \log \left[\frac{\mathbf{v}_i \cdot \mathbf{W}_i}{\mathbf{v}_i \cdot \boldsymbol{\mu}_\theta} \mu_{\theta j} \right] - \frac{\mathbf{v}_i \cdot \mathbf{W}_i}{\mathbf{v}_i \cdot \boldsymbol{\mu}_\theta} \mu_{\theta j} \right) \right] \quad (14)$$

$$\mathbb{E}_{\mathbf{W}, \mathbf{X}, \Gamma} \mathbb{E}_{\mathbf{W} | \mathbf{W}, \mathbf{X}, \Gamma} \left[\sum_{j=1}^J v_{ij} \left(W_{ij} \log \left[\frac{\mathbf{v}_i \cdot \mathbf{W}_i}{\mathbf{v}_i \cdot \boldsymbol{\mu}_\theta} \mu_{\theta j} \right] - \frac{\mathbf{v}_i \cdot \mathbf{W}_i}{\mathbf{v}_i \cdot \boldsymbol{\mu}_\theta} \mu_{\theta j} \right) \right] \quad (15)$$

$$= \mathbb{E}_{\mathbf{W}, \mathbf{X}, \Gamma} \left[\sum_{j=1}^J v_{ij} W_{ij} \log \mathbf{v}_i \cdot \mathbf{W}_i \right] \quad (16)$$

$$+ \mathbb{E}_{\mathbf{W}, \mathbf{X}, \Gamma} \left[\sum_{j=1}^J v_{ij} \left(W_i \cdot \frac{\mu_{\theta_0 j}}{\mu_{\theta_0}} \log \frac{\mu_{\theta j}}{\mathbf{v}_i \cdot \boldsymbol{\mu}_\theta} - W_i \cdot \frac{\mathbf{v}_i \cdot \boldsymbol{\mu}_{\theta_0}}{\mu_{\theta_0}} \frac{\mu_{\theta j}}{\mathbf{v}_i \cdot \boldsymbol{\mu}_\theta} \right) \right] \quad (17)$$

$$= C + \mathbb{E}_{\mathbf{W}, \mathbf{X}, \Gamma} \left[W_i \cdot \frac{\mathbf{v}_i \cdot \boldsymbol{\mu}_{\theta_0}}{\mu_{\theta_0}} \sum_{j=1}^J v_{ij} \left(\frac{\mu_{\theta_0 j}}{\mathbf{v}_i \cdot \boldsymbol{\mu}_{\theta_0}} \log \frac{\mu_{\theta j}}{\mathbf{v}_i \cdot \boldsymbol{\mu}_\theta} - \frac{\mu_{\theta j}}{\mathbf{v}_i \cdot \boldsymbol{\mu}_\theta} \right) \right] \quad (18)$$

We note that the term in line 5 above depends on θ_0 but not θ ; accordingly, we represent it with constant C on line 7.

9.3 Optimizer of profile likelihood

We now show that, under a suitable identifiability condition, a weak condition on \mathbf{W} , and a condition on weighting function v , that if $\mathbb{E}[\mathbf{W} | \mathbf{X}, \Gamma] = \exp(\Gamma) \boldsymbol{\mu}_{\theta_0}(\mathbf{X})$, then the unique optimizer of population criterion $M^v(\theta)$ is θ_0 .

The additional conditions we need are as follows:

- (D) For all $\theta, \theta' \in \Theta$, we have that, for any $a \in \mathbb{R}^+$, $\theta \neq \theta' \Rightarrow \boldsymbol{\mu}_\theta(\mathbf{x}) \neq a \boldsymbol{\mu}_{\theta'}(\mathbf{x})$ holds for all $\mathbf{x} \in A \subset \mathcal{X}$ with $P_{\mathbf{X}}(A) > 0$.
- (E) Weighting function $v : \mathcal{X} \times \mathcal{W} \rightarrow \mathbb{R}_{>0}^J$, where \mathcal{W} is the support of W , is continuous and bounded.

We will use the following simple lemma:

Lemma 1: For every $a \geq 0$, the function defined by $f_a(b) := a \log(b) - b$ is uniquely maximized at $b = a$ (defining $0 \log 0 := 0$ and letting $a \log 0 = -\infty$ for every $a > 0$).

Proof: First consider the case $a > 0$. Since $f_a(0) = -\infty$ in this case and f_a is finite for all $b > 0$, the optimum cannot occur at $b = 0$. Over $b \in \mathbb{R}^+$, $\frac{\partial^2}{\partial b^2} f = -\frac{a}{b^2} < 0$, so f_a is strictly convex over \mathbb{R}^+ and hence takes a unique optimum. Setting $\frac{\partial}{\partial b} f = \frac{a}{b} - 1 = 0$ gives us that the optimum occurs at $b = a$.

When $a = 0$, $f_a(b) = \begin{cases} 0 & \text{if } b = 0 \\ -b & \text{if } b > 0 \end{cases}$, so f_a is optimized at 0 since $-b < 0$ when $b > 0$.

Theorem 1: Suppose that conditions (A) - (D) are met. Then for any weighting function satisfying (E), the criterion $M^v(\cdot)$ defined above is uniquely optimized at θ_0 .

Proof: From above we have the form of the population criterion $M^v(\theta)$:

$$M^v(\theta) = C + \mathbb{E}_{\mathbf{W}, \mathbf{x}, \Gamma} \left[W \cdot \frac{\mathbf{v} \cdot \boldsymbol{\mu}_{\theta_0}}{\mu_{\theta_0 \cdot}} \sum_{j=1}^J v_{ij} \left(\frac{\mu_{\theta_0 j}}{\mathbf{v}_i \cdot \boldsymbol{\mu}_{\theta_0}} \log \frac{\mu_{\theta j}}{\mathbf{v}_i \cdot \boldsymbol{\mu}_{\theta}} - \frac{\mu_{\theta j}}{\mathbf{v}_i \cdot \boldsymbol{\mu}_{\theta}} \right) \right] \quad (19)$$

For each fixed $\mathbf{x} \in \mathcal{X}$,

$$h_j^v(x, \theta; \theta_0) := \frac{\mu_{\theta_0 j}}{\mathbf{v}_i \cdot \boldsymbol{\mu}_{\theta_0}}(\mathbf{x}) \log \frac{\mu_{\theta j}}{\mathbf{v}_i \cdot \boldsymbol{\mu}_{\theta}}(\mathbf{x}) - \frac{\mu_{\theta j}}{\mathbf{v}_i \cdot \boldsymbol{\mu}_{\theta}}(\mathbf{x}) \quad (20)$$

is maximized when $\frac{\mu_{\theta j}}{\mathbf{v}_i \cdot \boldsymbol{\mu}_{\theta}}(\mathbf{x}) = \frac{\mu_{\theta_0 j}}{\mathbf{v}_i \cdot \boldsymbol{\mu}_{\theta_0}}(\mathbf{x})$ by Lemma 1.

Before proceeding, we show that $-\infty < M^v(\theta_0) < \infty$. By definition, we have

$$M^v(\theta_0) = \mathbb{E}_{\mathbf{W}, \mathbf{x}, \Gamma} \sup_{\gamma \in \mathbb{R}} \sum_{j=1}^J v_j (W_j \log [\exp(\gamma) \frac{\mathbf{v} \cdot \mathbf{W}}{\mathbf{v} \cdot \boldsymbol{\mu}_{\theta_0}} \mu_{\theta_0 j}] - \exp(\gamma) \frac{\mathbf{v} \cdot \mathbf{W}}{\mathbf{v} \cdot \boldsymbol{\mu}_{\theta_0}} \mu_{\theta_0 j}) \quad (21)$$

$$\geq \mathbb{E}_{\mathbf{W}, \mathbf{x}, \Gamma} \sum_{j=1}^J v_j (W_j \log [\frac{\mathbf{v} \cdot \mathbf{W}}{\mathbf{v} \cdot \boldsymbol{\mu}_{\theta_0}} \mu_{\theta_0 j}] - \frac{\mathbf{v} \cdot \mathbf{W}}{\mathbf{v} \cdot \boldsymbol{\mu}_{\theta_0}} \mu_{\theta_0 j}) \quad (\text{setting } \gamma = 0) \quad (22)$$

$$= \mathbb{E}_{\mathbf{W}, \mathbf{x}, \Gamma} \sum_{j=1}^J v_j W_j \log \mathbf{v} \cdot \mathbf{W} \quad (23)$$

$$+ \mathbb{E}_{W, \mathbf{x}, \Gamma} \frac{\mathbf{v} \cdot \boldsymbol{\mu}_{\theta_0}}{\mu_{\theta_0 \cdot}} W \cdot \sum_{j=1}^J \left[\frac{\mu_{\theta_0 j}}{\mathbf{v} \cdot \boldsymbol{\mu}_{\theta_0}} \log \frac{\mu_{\theta_0 j}}{\mathbf{v} \cdot \boldsymbol{\mu}_{\theta_0}} - \frac{\mu_{\theta_0 j}}{\mathbf{v} \cdot \boldsymbol{\mu}_{\theta_0}} \right] \quad (24)$$

The term in line (23) is equal to $\mathbb{E}_{\mathbf{W}, \mathbf{X}, \Gamma} \mathbf{v} \cdot \mathbf{W} \log \mathbf{v} \cdot \mathbf{W}$, which as the integral of a bounded function over a bounded domain is finite. By assumption (C), we must have $\sum_j \mu_{\theta_{0j}}(\mathbf{X}) > 0$ almost surely, so the front term in line (24) is almost surely bounded by boundedness of μ_θ and v . Inside the sum in this line, we have terms of the form $a \log a - a$, which is a bounded function on any bounded set in $\mathbb{R}_{\geq 0}$. Hence line (24) is an integral of a bounded function over a bounded domain and so is also finite, so $M^v(\theta_0) > -\infty$.

Similarly,

$$M^v(\theta_0) = \mathbb{E}_{\mathbf{W}, \mathbf{X}, \Gamma} \sup_{\gamma \in \mathbb{R}} \sum_{j=1}^J v_j (W_j \log [\exp(\gamma) \frac{\mathbf{v} \cdot \mathbf{W}}{\mathbf{v} \cdot \boldsymbol{\mu}_{\theta_0}} \mu_{\theta_{0j}}] - \exp(\gamma) \frac{\mathbf{v} \cdot \mathbf{W}}{\mathbf{v} \cdot \boldsymbol{\mu}_{\theta_0}} \mu_{\theta_{0j}}) \quad (25)$$

$$\leq \mathbb{E}_{\mathbf{W}, \mathbf{X}, \Gamma} \sum_{j=1}^J v_j (W_j \log W_j - W_j) \text{ by lemma 1} \quad (26)$$

$$< \infty \text{ since } \sum_{j=1}^J v_j (W_j \log W_j - W_j) \text{ is bounded on } \mathcal{W} \times \mathcal{X} \times \mathcal{G} \quad (27)$$

Hence $-\infty < M^v(\theta_0) < \infty$, which guarantees that the difference in the following argument is not of the form $\infty - \infty$.

Now, for any $\theta \in \Theta$ with $\theta \neq \theta_0$, we have

$$\begin{aligned} & M^v(\theta) - M^v(\theta_0) \\ &= \int_A g(\mathbf{x}) \int \int w \frac{\mathbf{v} \cdot \boldsymbol{\mu}_{\theta_0}}{\mu_{\theta_0 \cdot}} \sum_{j=1}^J [h_j^v(\mathbf{x}, \theta; \theta_0) - h_j^v(\mathbf{x}, \theta_0; \theta_0)] dP_{W|\Gamma, \mathbf{X}}(w) dP_{\Gamma|\mathbf{X}}(\gamma) dP_{\mathbf{X}}(\mathbf{x}) \\ &+ \int_{A^c} \int \int w \frac{\mathbf{v} \cdot \boldsymbol{\mu}_{\theta_0}}{\mu_{\theta_0 \cdot}} \sum_{j=1}^J [h_j^v(\mathbf{x}, \theta; \theta_0) - h_j^v(\mathbf{x}, \theta_0; \theta_0)] dP_{W|\Gamma, \mathbf{X}}(w) dP_{\Gamma|\mathbf{X}}(\gamma) dP_{\mathbf{X}}(\mathbf{x}) \\ &\leq \int_A \int \int w \frac{\mathbf{v} \cdot \boldsymbol{\mu}_{\theta_0}}{\mu_{\theta_0 \cdot}} \sum_{j=1}^J [h_j^v(\mathbf{x}, \theta; \theta_0) - h_j^v(\mathbf{x}, \theta_0; \theta_0)] dP_{W|\Gamma, \mathbf{X}}(w) dP_{\Gamma|\mathbf{X}}(\gamma) dP_{\mathbf{X}}(\mathbf{x}) \quad (\star) \\ &< 0 \end{aligned}$$

The first inequality is a result of θ_0 maximizing (not necessarily uniquely) h_j^v ; i.e., $h_j^v(\mathbf{x}, \theta; \theta_0) - h_j^v(\mathbf{x}, \theta_0; \theta_0) \leq 0$. Strict inequality holds in the last line because the integrand in (\star) is strictly negative, since $h_j^v(\mathbf{x}, \theta; \theta_0) - h_j^v(\mathbf{x}, \theta_0; \theta_0) < 0$ for $\theta \neq \theta_0$ on A , and the front term $w \frac{\mathbf{v} \cdot \boldsymbol{\mu}_{\theta_0}}{\mu_{\theta_0 \cdot}}$ is a.s. strictly positive by assumption (C) and positivity of \mathbf{v} . Hence $M^v(\theta_0) > M^v(\theta)$ for all $\theta \neq \theta_0$ in Θ , so θ_0 is the unique maximizer of the population criterion $M^v(\cdot)$.

9.4 Consistency of M-estimators

We apply theorem 5.14 of van der Vaart (1998) to show consistency of maximizers $\hat{\theta}_n^v$ of M_n^v for θ_0 . We also show consistency of estimators $\hat{\theta}_n^{\hat{v}_n}$, where $\{\hat{v}_n\}$ is a sequence of random continuous positive bounded weighting functions converging uniformly in probability to v .

We first require the following assumption on v and \hat{v}_n :

(F) $\sup_{t \in \mathcal{X} \times \mathcal{W}} |v(t) - \hat{v}_n(t)| \xrightarrow{P} 0$ and every \hat{v}_n is positive and bounded.

Theorem 2

Suppose conditions (A) through (F) are satisfied. Then $Pr(d(\hat{\theta}^v, \theta_0) > \epsilon) \rightarrow 0$ for all $\epsilon > 0$ and $Pr(d(\hat{\theta}^{\hat{v}_n}, \theta_0) > \epsilon) \rightarrow 0$ for all $\epsilon > 0$ where $d(\cdot, \cdot)$ is given by $d(s, t) := \sum_k |\arctan s_k - \arctan t_k|$.

Proof

We first compactify our parameter space Θ to obtain $\bar{\Theta}$ by allowing elements of unconstrained Euclidean parameters to take values in the extended reals.

A necessary condition for theorem 5.14 is that we have $P \sup_{\theta \in U} m_\theta^v < \infty$ for $m_\theta^v(\mathbf{w}) := \sum_{j=1}^J v_j(w_j \log[\frac{\mathbf{v} \cdot \mathbf{w}}{\mathbf{v} \cdot \mu_\theta} \mu_{\theta_j}] - \frac{\mathbf{v} \cdot \mathbf{w}}{\mathbf{v} \cdot \mu_\theta} \mu_{\theta_j})$ and a sufficiently small ball $U \in \Theta$. By lemma 1, $\sup_{\theta \in U} m_\theta^v(\mathbf{w}) \leq \sum_{j=1}^J v_j(w_j \log w_j - w_j)$, which is bounded above since v is bounded. Hence by assumption (A), $P \sup_{\theta \in U} m_\theta^v \leq P \sum_{j=1}^J v_j(w_j \log w_j - w_j) < \infty$. We also require $M_n^v(\hat{\theta}^v) = M_n^v(\theta_0) + o_P(1)$ which is trivially satisfied since $\hat{\theta}^v$ maximizes M_n^v .

Then letting compact set $K = \bar{\Theta}$, we can directly apply theorem 5.14 to obtain $Pr(d(\hat{\theta}^v, \theta_0) \geq \epsilon) \rightarrow 0$ for any $\epsilon > 0$.

To apply theorem 5.14 to $\hat{\theta}_n^{\hat{v}_n}$, we only need in addition to the above that $M_n^v(\hat{\theta}_n^{\hat{v}_n}) = M_n^v(\theta_0) + o_P(1)$.

For any fixed \hat{v} , we have

$$M_n^{\hat{v}}(\hat{\theta}_n^{\hat{v}}) = M_n^{\hat{v}}(\theta_0) + o_P(1) \tag{28}$$

$$= M_n^v(\theta_0) + o_P(1) + (M_n^v(\theta_0) - M_n^{\hat{v}}(\theta_0)) \tag{29}$$

However, the term $(M_n^v(\theta_0) - M_n^{\hat{v}}(\theta_0)) = o_P(1)$ if we let $\hat{v} = \hat{v}_n$ since

$$|M_n^{\hat{v}_n}(\theta_0) - M_n^v(\theta_0)| = \left| \frac{1}{n} \sum_{i=1}^n \sum_{j=1}^J (\hat{v}_{n,ij} - v_{ij}) l_{ij}(\theta_0) \right| \quad (30)$$

$$\leq \sup_{t \in \mathcal{X} \times \mathcal{W}} |\hat{v}_n(t) - v(t)| \frac{1}{n} \sum_{i=1}^n \sum_{j=1}^J |l_{ij}(\theta_0)| \xrightarrow{P} 0 \quad (31)$$

since $\sup_{t \in \mathcal{X} \times \mathcal{W}} |\hat{v}_n(t) - v(t)| \xrightarrow{P} 0$. Hence $M_n^v(\hat{\theta}^{\hat{v}_n}) = M_n^v(\theta_0) + o_P(1)$, so $Pr(d(\hat{\theta}^{\hat{v}_n}, \theta_0) \geq \epsilon) \rightarrow 0$ for any $\epsilon > 0$.

9.5 Convergence in distribution of M-estimators

In this section we provide a brief sketch of convergence results for $\sqrt{n}(\hat{\theta}_n^v - \theta_0)$. Letting \mathbb{P}_n denote the empirical distribution function of n independent pairs $(\mathbf{W}_i, \mathbf{X}_i)$, with each pair taking values in some subset of \mathbb{R}^d and with P the true distribution for (\mathbf{W}, \mathbf{X}) , we have

$$\sqrt{n}(\mathbb{P}_n - P) \rightsquigarrow \mathbb{G}_P \quad (32)$$

in $l^\infty(P)$ for Gaussian process \mathbb{G}_P . Letting $g(P) := \arg \max_{\theta \in \Theta} P m_\theta^v$, if g has Hadamard directional derivative \dot{g} at P , then we can apply the infinite dimensional delta method (Römisch, 2004) to obtain

$$\sqrt{n}(g(\mathbb{P}_n) - g(P)) = \sqrt{n}(\hat{\theta}_n^v - \theta_0) \rightsquigarrow \dot{g}(\mathbb{G}_P) \quad (33)$$

Using weights \hat{v}_n estimated from data does not affect convergence, as we have

$$\sqrt{n}(M_n^{\hat{v}_n}(\theta) - M^{\hat{v}_n}(\theta)) \quad (34)$$

$$= \sqrt{n}(M_n^v(\theta) - M^v(\theta) + [M_n^{\hat{v}_n}(\theta) - M_n^v(\theta)] - [M^{\hat{v}_n}(\theta) - M^v(\theta)]) \quad (35)$$

$$= \sqrt{n}(M_n^v(\theta) - M^v(\theta)) + \sqrt{n}(\mathbb{P}_n - P) m_\theta^{\hat{v}_n - v} \quad (36)$$

$$= \sqrt{n}(M_n^v(\theta) - M^v(\theta)) + o_P(1) \quad (37)$$

since

$$\sqrt{n}(\mathbb{P}_n - P)m_{\hat{\theta}}^{\hat{v}_n - v} = \sqrt{n} \frac{1}{n} \sum_{i=1}^n \sum_{j=1}^J (\hat{v}_{n;ij} - v_{ij}) l_{ij}(\theta) \quad (38)$$

$$\leq \sqrt{n} \frac{1}{n} \sum_{i=1}^n \sum_{j=1}^J |l_{ij}(\theta)| \sup_{t \in \mathcal{W} \times \mathcal{X}} |\hat{v}_n(t) - v(t)| \quad (39)$$

$$\xrightarrow{p} 0 \quad (40)$$

Note that $\arg \max_{\theta \in \Theta} M^{\hat{v}_n}(\theta) = \arg \max_{\theta \in \Theta} M^v(\theta) = \theta_0$ by theorem 1.

10 Optimization details

10.1 Reparametrization of barrier subproblem

Letting θ^* indicate the unknown parameters in our model after reparametrizing \mathbf{p} and $\tilde{\mathbf{p}}$ as $\boldsymbol{\rho}$ and $\tilde{\boldsymbol{\rho}}$, we now have the following unconstrained minimization problem:

$$\arg \min_{\theta^*} f_n(\theta^*) + \frac{1}{t^{(r)}} \left[\sum_k \left(\sum_{j=1}^{J-1} -\rho_{kj} + J \log \left[1 + \sum_{j=1}^{J-1} \exp(\rho_{kj}) \right] \right) \right] \quad (41)$$

$$\sum_{\tilde{k}} \left(\sum_{j=1}^{J-1} -\tilde{\rho}_{\tilde{k}j} + J \log \left[1 + \sum_{j=1}^{J-1} \exp(\tilde{\rho}_{\tilde{k}j}) \right] \right) \right] \quad (42)$$

10.2 Barrier algorithm

Barrier Algorithm

1. Initiate with value of penalty parameter t set to starting value $t^{(0)}$ and values of parameters θ^* equal to $\theta^{*(0)}$. Set iteration $r = 0$.
2. Using current value $t^{(r)}$ of t and starting at parameter estimate $\theta^{*(r)}$, solve barrier subproblem r given above via Fisher scoring. Denote the solution of this subproblem $\theta_{(r+1)}^*$ and set $t_{(r+1)} = at_{(r)}$ for a prespecified $a > 1$.
3. If $t_{(r+1)} > t_{\max}$ for prespecified t_{\max} , return $\theta_{(r+1)}^*$. Otherwise set iteration $r = r + 1$ and return to step 2.

10.3 Constrained Newton within Augmented Lagrangian Algorithm

We calculate update steps from \mathcal{L}_k given in Section 3 of the main text as follows:

Constrained Newton within Augmented Lagrangian Algorithm

1. Initiate with initial values $\nu^{(0)}$ and $\mu^{(0)} > 0$ of penalty coefficients ν and μ
2. Calculate proposed update $\mathbf{p}_k^{\text{update}}$ via nonnegative least squares on \mathcal{L}_k using current values of ν and μ
3. If $|\sum_j^J p_{kj}^{\text{update}} - 1| < \delta$ for some prespecified tolerance $\delta > 0$, set update direction $\mathbf{s}_k := \mathbf{p}_k - \mathbf{p}_k^{\text{update}}$ and proceed to step (3). Otherwise update ν and μ via algorithm given in Bazaraa (2006) (p. 496) and return to step (1).
4. Perform a line search in direction \mathbf{s}_k to determine updated parameter value $\mathbf{p}_k^{\text{updated}} := \mathbf{p}_k + \epsilon \mathbf{s}_k$ that decreases $f_n(\mathbf{p}_k)$ for some $0 < \epsilon \leq 1$.

10.4 Quadratic approximation to $f_n(\mathbf{p}_k)$.

In Section 3 of the main text, we specify \mathcal{L}_k in terms of a quadratic approximation $Q_k^{(t)}$ to objective $f_n(\mathbf{p}_k)$. In practice we construct $Q_k^{(t)}$ as a slightly modified Taylor expansion of $f_n()$ around the current value of $\mathbf{p}_k^{(t)}$. We use the gradient of f_n with respect to \mathbf{p}_k in the first order term, and in the second order term, and in place of the Hessian, we use (-1 times) the Fisher information matrix in \mathbf{p}_k regularized (for numerical stability) by addition of magnitude of the gradient times an identity matrix.

11 Analysis of Costea et al. (2017) data

11.1 Details of model specification

Costea et al. (2017) published two flow cytometric readings for every species in the synthetic community with the exception of *V. cholerae*, for which only one reading was published. In all taxa save *V. cholerae*, we take the mean reading as our observation, and we include the resulting vector of readings augmented by the single reading for *V. cholerae* as a row in \mathbf{W} . We anticipate that our use of mean readings represents a fairly small loss of information, as flow cytometric readings did not vary substantially within taxon. However, in a similar setting where multiple sets of flow cytometric readings across all taxa were available, we could include each set as a row of \mathbf{W} to capture variability in these measurements.

To estimate detection effects relative to flow cytometry measurements, we specify $X_1 = \mathbf{0}$. For $i \geq 2$, $\mathbf{X}_i = [1 \ \mathbf{1}_Q \ \mathbf{1}_W]$ where $\mathbf{1}_Q$ is an indicator for sample i being processed according to protocol Q, and similarly for $\mathbf{1}_W$.

11.2 Cross-validation design

We construct folds for our 10-fold cross-validation on Costea et al. (2017) data so that, with the exception of samples A and B, which we grouped together in a single fold, each fold included all observations for a given specimen. For each fold, we fit a model in which all observations in all

other folds, along with flow cytometry readings, were treated as arising from a common specimen (as in fact they do, save for flow cytometry readings, which were taken on specimens mixed to create the mock spike-in). We model each sample in the held-out fold as arising from a distinct specimen of unknown composition to allow our model to estimate a different relative abundance profile for distinct samples processed according to different protocols.

11.3 Model summaries

Table 1: Point estimates and 95% bootstrap confidence intervals for protocol-specific detection effects β (with reference taxon *Y. pseudotuberculosis*) estimated from Costea et al. (2017) data

Taxon	Protocol H	Protocol Q	Protocol W
<i>B. hansenii</i>	-1.61 (-2.00 – -1.16)	-1.55 (-1.75 – -1.31)	-0.08 (-0.16 – 0.00)
<i>C. difficile</i>	-0.18 (-0.30 – 0.01)	-0.57 (-0.79 – -0.41)	1.23 (1.18 – 1.28)
<i>C. perfringens</i>	3.38 (3.27 – 3.57)	2.48 (2.31 – 2.62)	4.05 (4.03 – 4.07)
<i>C. saccharolyticum</i>	-0.19 (-0.23 – -0.16)	-0.01 (-0.12 – 0.1)	-0.10 (-0.13 – -0.06)
<i>F. nucleatum</i>	2.37 (2.28 – 2.44)	0.14 (-0.16 – 0.42)	2.11 (2.05 – 2.16)
<i>L. plantarum</i>	-2.62 (-2.96 – -2.12)	0.72 (0.60 – 0.93)	0.60 (0.56 – 0.63)
<i>P. melaninogenica</i>	4.17 (4.12 – 4.2)	3.88 (3.82 – 4.04)	4.25 (4.23 – 4.27)
<i>S. enterica</i>	2.49 (2.45 – 2.51)	2.74 (2.64 – 2.79)	2.48 (2.46 – 2.51)
<i>V. cholerae</i>	1.54 (1.50 – 1.56)	0.90 (0.78 – 0.99)	1.48 (1.44 – 1.50)

Table 1 provides point estimates and marginal 95% confidence intervals for the detection effects for each of protocols H, Q, and W estimated via the full model described above. This model was fit with reference taxon *Y. pseudotuberculosis* (i.e., under the constraint that the column of β corresponding to this taxon consists of 0 entries). Hence we interpret estimates in this table in terms of degree of over- or under-detection relative to *Y. pseudotuberculosis* – for example, we estimate that, repeated measurement under protocol H of samples consisting of 1:1 mixtures of *B. hansenii* and *Y. pseudotuberculosis*, the mean MetaPhlAn2 estimate (under the settings used by

McLaren et al. (2019)) of the relative abundance of *B. hansenii* will be $\exp(-1.61) \approx 0.20$ as large as the mean estimate of the relative abundance of *Y. pseudotuberculosis*.

12 Analysis of Karstens et al. (2019) data

12.1 Preprocessing

We process raw read data reported by Karstens et al. (2019) using the DADA2 R package (version 1.20.0) (Callahan et al., 2016). We infer amplicon sequence variants using the *dada* function with option ‘pooled = TRUE’ and assign taxonomy with the *assignSpecies* function using a SILVA v138 training dataset downloaded from <https://benjjneb.github.io/dada2/training.html> (Quast et al., 2012).

12.2 Model Specification

We conduct a three-fold cross-validation of a model containing both contamination and detection effects. For each held-out fold r , if we let $\mathbf{e}_r := (\mathbf{1}_{[\text{sample 1 in fold } r]}, \dots, \mathbf{1}_{[\text{sample } n \text{ in fold } r]})^T$, $\mathbf{d} = (3^0, \dots, 3^8)^T$, and \circ indicate element-wise multiplication then we specify the model for this fold with

$$\begin{aligned}\mathbf{Z} &= \begin{bmatrix} \mathbf{1} - \mathbf{e}_r & \mathbf{e}_r \end{bmatrix} \\ \tilde{\mathbf{Z}} &= \begin{bmatrix} \mathbf{d} \circ (\mathbf{1} - \mathbf{e}_r) \end{bmatrix} + \exp(\tilde{\alpha}) \begin{bmatrix} \mathbf{d} \circ \mathbf{e}_r \end{bmatrix} \\ \mathbf{X} &= \vec{\mathbf{1}} \\ \tilde{\mathbf{X}} &= \mathbf{0}\end{aligned}$$

The relative abundance matrix \mathbf{p} consists of two rows, the first of which is treated as fixed and known and contains the theoretical composition of the mock community used by Karstens et al. (2019). The second row is to be estimated from observations on samples in the held-out fold. $\tilde{\mathbf{p}}$ consists of a single row, the first 247 elements of which we treat as unknown. We fix $\tilde{p}_{248} = 0$ as an identifiability constraint – identifiability problems arise here because all samples sequenced arise from the same specimen, we lack identifiability over, for any choice of fixed $\tilde{\mathbf{p}}^*$ and \mathbf{p} , the set

$\{\tilde{\mathbf{p}} = a * \tilde{\mathbf{p}}^* + (1 - a)\mathbf{p} : 0 \leq a \leq 1\}$. Briefly, we do not consider the assumption $\tilde{p}_{248} = 0$ unrealistic; while in general distinguishing between contaminant and non-contaminant taxa is challenging, it is fairly frequently the case that choosing a single taxon *unlikely* to be a contaminant is not difficult. Moreover, we anticipate that in most applied settings, more than one specimen will be sequenced and this identifiability problem will hence not arise.

β consists of a single row, the first $J - 8 = 240$ elements of which (corresponding to contaminant taxa) are treated as fixed and known parameters equal to 0, as we cannot estimate detection efficiencies in contaminant taxa. The following 7 elements of β are treated as fixed and unknown (to be estimated from data), and the 248th element of β is set equal to 0 as an identifiability constraint. $\tilde{\gamma}$ is specified as a single unknown parameter in \mathbb{R}

The full model fit without detection efficiencies β is specified by treating β as fixed and known with all elements equal to 0. We treat all samples as arising from the same specimen, so $\mathbf{Z} = \mathbf{1}$, $\tilde{\mathbf{Z}} = \mathbf{d}$, and \mathbf{p} consists of a single row treated as an unknown relative abundance. Specifications of \mathbf{X} , $\tilde{\mathbf{X}}$, $\tilde{\mathbf{p}}$, and $\tilde{\gamma}$ do not differ from above.

12.3 Additional summaries

Table 2: Entries of $\hat{\beta}$ (reference taxon *L. fermentum*) estimated from Karstens et al. (2019) data

Taxon	Estimate
<i>P. aeruginosa</i>	-1.29
<i>E. coli</i>	-0.20
<i>S. enterica</i>	-0.48
<i>E. faecium</i>	-2.09
<i>S. aureus</i>	-3.05
<i>L. monocytogenes</i>	-1.60
<i>B. halotolerans</i>	-0.74

For each taxon for which β_j is identifiable (i.e., taxa in the mock community), our model produces a point estimate $\hat{\beta}_j$, as show in table 2 above. (The reference taxon, *L. fermentum*, for which we

enforce identifiability constraint $\beta_j = 0$, is excluded.) On the basis of this model, we estimate that in an equal mixture of *E. coli* and our reference taxon, *L. fermentum* sequenced by the method used by Karstens et al. (2019), we expect on average to observe $\exp(-0.20) \approx 0.82$ *E. coli* reads for each *L. fermentum* read. In an equal mixture of *S. aureus* and *L. fermentum* similarly sequenced, we expect on average to observe $\exp(-3.05) \approx 0.047$ reads for each *L. fermentum* read. As only two samples were treated as known in our analysis, we do not attempt to quantify uncertainty around these point estimates.

13 Simulation results based on Brooks et al. (2015) data

13.1 Identifiability

In our simulation using Brooks et al. (2015) data, we repeatedly selected sets of 3, 5, 10, or 20 samples from each of two plates of 40 samples sequenced by Brooks et al. (2015) to treat as known. For each randomly selected subset of samples to be treated as known, we required that β be identifiable on the basis of the taxa present in all known samples on each plate (i.e., identifiable from either group of samples). Briefly, this amounts to requiring that the graph whose nodes are the 7 taxa under consideration with edges between two nodes if the taxa those nodes correspond to are present in the same known sample. When a randomly selected set of samples failed this requirement, we redrew sets of samples until we found one that satisfied it.

13.2 Figures

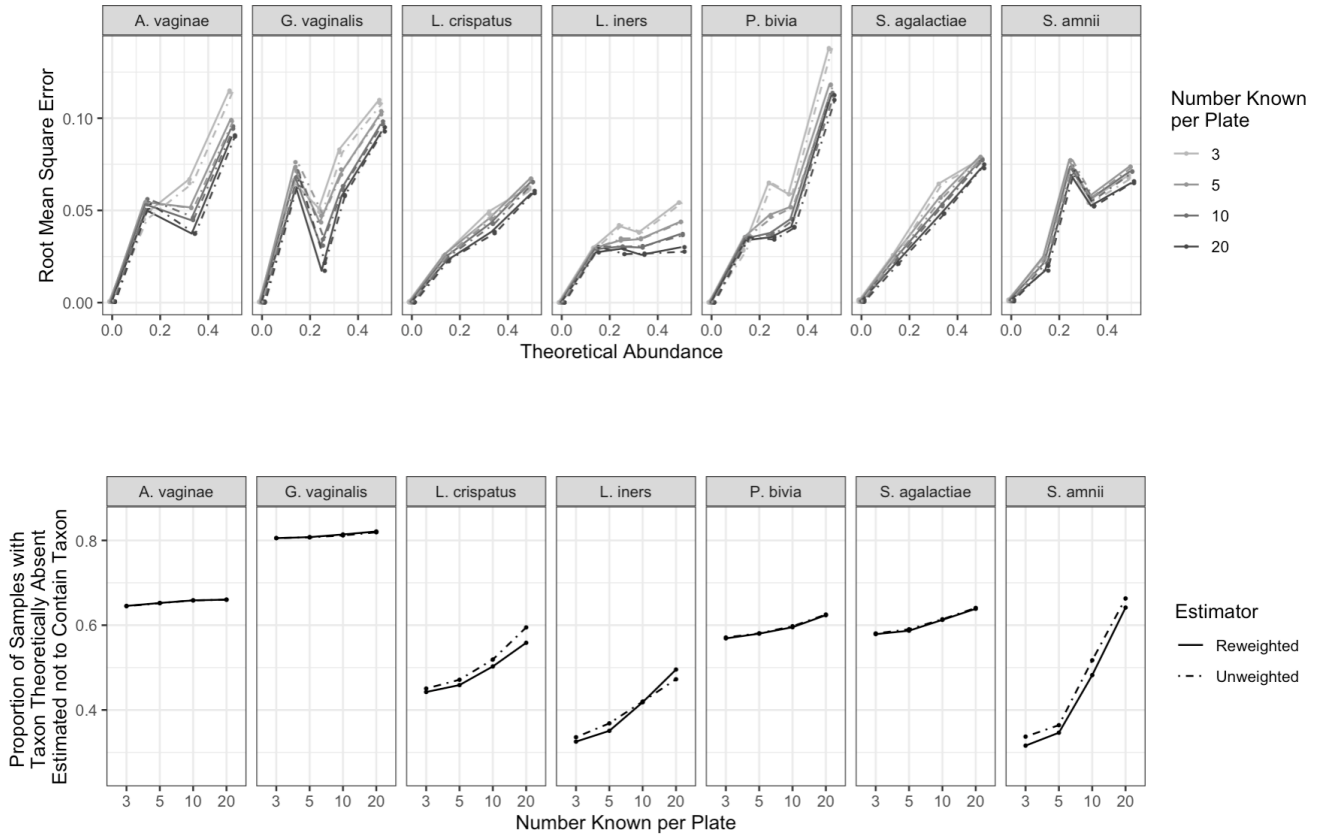


Figure 4: Predictive performance of models fit on Brooks et al. (2015) data. The upper row includes root mean square error of relative abundance estimates by estimator, taxon, number of samples treated as known per plate, and true relative abundance. True relative abundance is given on the x-axis and root mean square error is plotted on the y-axis; for concision, true relative abundances equal to 1 are plotted at 0. Each column pane contains estimates for a different taxon, estimator is indicated with line type (solid for Poisson and dashed for weighted Poisson), and number of samples known per plate is indicated by color. In the lower row, proportion of elements of \mathbf{P} truly equal to zero estimated to be equal to zero is plotted on the y-axis of each pane, and the x-axis gives number of samples per plate treated as known. Taxon and estimator are represented as in the upper row, and the proportion of nonzero elements of \mathbf{W} corresponding to zero elements of \mathbf{P} for each taxon is plotted as a dotted horizontal line.